Review of ten years of volcano deformations recorded by the ground-based InSAR monitoring system at Stromboli volcano: a tool to

Earth-Science Reviews 139 (2014) 317–335

Contents lists available at ScienceDirect

Earth-Science Reviews

journal homepage: www.elsevier.com/locate/earscirev

Review of ten years of volcano deformations recorded by the ground-based InSAR monitoring system at Stromboli volcano: a tool to mitigate volcano flank dynamics and intense volcanic activity

Federico Di Traglia [a,b], Teresa Nolesini [a,*], Emanuele Intrieri [a], Francesco Mugnai [a], Davide Leva [c], Mauro Rosi [b], Nicola Casagli [a]

[a] Dipartimento di Scienze della Terra, Università di Firenze, Via La Pira 4, Firenze, Florence, Italy
[b] Dipartimento di Scienze della Terra, Università di Pisa, Via Santa Maria 53, Pisa, Italy
[c] Ellegi s.r.l. – LiSALab, via Petrarca 55, Rovello Porro, Como, Lombardy, Italy

ARTICLE INFO

Article history:
Received 10 April 2014
Accepted 26 September 2014
Available online 6 October 2014

Keywords:
Volcano deformation
GBInSAR
Volcano monitoring
Stromboli volcano
Flank volcano dynamics
Tsunamogenic landslide

ABSTRACT

Stromboli volcano (Southern Italy) is one of the most monitored volcano in the world with a surveillance network that includes a permanently sited ground-based SAR interferometer (GBInSAR). This work is the review of the GBInSAR data gained from the last decade of monitoring activity. The analysis of the entire dataset of GBInSAR measurements allowed the assessment of the deformation field of the northern part of the summit crater area and the Sciara del Fuoco depression. In detail, the main displacements recognized can be related to different factors: 1) the inflation/deflation respectively immediately before and after each new effusive event; 2) the bulging of localized sectors of the volcano involved in the vent opening; 3) the gravitational sliding of the Sciara del Fuoco infill; 4) the movement of lava flows. Accelerations in this sector are related to sheet intrusions, while the possibility of vent opening, associated with small sliding, or catastrophic flank failure are related to highly overpressurized sheets, able to produce high displacement rate in the Sciara del Fuoco.

In the summit crater area, the increases in the displacement rate are related to the pressurization of the shallow conduit system, as the consequence of the variation in the magma level (magmastatic pressure) or to the lateral magma migration (lateral conduit expansion or dike intrusion) in response to the increase of the overpressure component. Fluctuations in the displacement rate in the summit crater area can be related to the magma overturning within the conduit, with the increases in displacement rate during the upwelling of less dense magma, while displacement rate decreases as the degassed magma column is pushed out from the conduit (lava flows or overflows). Instead, the decrease in the displacement rate without coeval lava outpouring could be related to the sink of the degassed magma due to density contrast between the gas-poor and the gas-charged magmas. Using the displacement rate in the summit crater area as a proxy for the variation in the pressure condition in conduit (both magmastatic and overpressure components), thresholds for the crises characterized by the occurrence of overflows (eventually associated with major explosions) and flank effusions (eventually associated with paroxysmal explosions) are identified. Small conduit overpressure will produce overflows (sometimes associated with crater-rim collapses), while large magma overpressure will laterally expand the conduit forming NE-SW striking sheets, feeding eruptive vents at the base of the summit crater area and within the Sciara del Fuoco, generating conditions of instability that can evolve into catastrophic collapse of the instable flank.

Contents

* Corresponding author.
E-mail address: teresa.nolesini@unifi.it (T. Nolesini).

http://dx.doi.org/10.1016/j.earscirev.2014.09.011

1. Introduction

Since the 2002–03 flank effusion, characterized by a tsunamogenic landslide provoked by the intrusion of a dyke in the Sciara del Fuoco (SdF), together with a paroxysmal explosion (Rosi et al., 2006; Neri et al., 2008), Stromboli became one of the most monitored volcano in the world with a progressive improvement of the surveillance network (Barberi et al., 2009), comprising 13 broadband digital seismometers (Giudicepietro et al., 2009), tiltmeters (Bonaccorso et al., 2009), an automated distance measuring station (Puglisi et al., 2005), a continuous GPS network (Mattia et al., 2004), two strainmeters (Bonaccorso et al., 2012), a network of visual and thermal cameras (Bonaccorso et al., 2012), magnetic and gravity stations (Carbone et al., 2012), a permanent side Ground-based Interferometric Synthetic Aperture Radar (GBInSAR; Antonello et al., 2004), 4 seismo-acoustic stations (Goto et al., 2014), a system of optical radiometers and infrared and visible light cameras and a geochemical network for the automatic monitoring of the SO_2 flux (Burton et al., 2009) and the CO_2/SO_2 ratio of the crater gas plume (Aiuppa et al., 2009), the CO_2 soil flux and the dissolved CO_2 in the thermal water wells (Inguaggiato et al., 2011). The GBInSAR is, so far, the only example in the literature of such technology applied to the surveillance of an active volcano. It is used for landslide monitoring in the area of the Sciara del Fuoco (Casagli et al., 2010; Intrieri et al., 2013; Nolesini et al., 2013), coupled with the automated distance measuring station (Bonforte et al., 2008), and for monitoring inflation-deflation of the summit crater area that can reveal any change in the volcanic activity (Casagli et al., 2009; Di Traglia et al., 2013, 2014a,b). It is considered as the best way to capture short, subtle episodes of conduit pressurization in open vent volcanoes like Stromboli (Chris Newhall, pers. comm.). Stromboli is an open-conduit volcano and does not experience pressurization of the magma storage and/or plumbing system that produces ground deformations at the scale of the volcanic edifice. For any such system, localized inflation or deflation may occur in response to conduit processes, such as magma convection and uprising (Bonaccorso and Davis, 1999; Chaussard et al., 2013). Detectable ground deformation at Stromboli has only been observed in association with dyke intrusion at shallow depth, prior to the opening of new eruptive fractures (Bonaccorso, 1998; Bonaccorso et al., 2008; Casagli et al., 2009).

Stromboli (Fig. 1) is one of the most well-known volcanoes in the world and its persistent activity, consisting of frequent, small scale, explosions gave its name to *Strombolian activity* (Blackburn et al., 1976). Intrusion-related landslides from the NW unstable flank of the volcano (the Sciara del Fuoco depression; Fig. 1b) are also frequent (Barberi et al., 1993; Di Roberto et al., 2008, 2010; Rosi et al., 2013) and are the most hazardous phenomena, due to their tsunamogenic potential (Fig. 2; Tinti et al., 2005; Nave et al., 2010; Nolesini et al., 2013). Tsunamis have occurred numerous times in recent centuries and can affect large areas of the coast of Stromboli (Barberi et al., 1993; Tinti et al., 2005; Rosi et al., 2013 and references therein). However, the most frequent hazards at Stromboli are related to the occurrence of higher-intensity Strombolian explosions (paroxysmal or major explosion, based on the scale of the main blast; Barberi et al., 1993). Paroxysmal events affected large zones and produced bombs and blocks that reached inhabited areas (mainly to Ginostra village in the SW part of the Island) and hot avalanches that caused fatalities (i.e. 1930 paroxysm; Bertagnini et al., 2011; Di Roberto et al., 2014).

Stromboli volcano is constantly erupting, with temporal and spatial changes in frequency, intensity, and nature of the activity (see, e.g., Taddeucci et al., 2013). Giving the persistent activity at Stromboli, we prefer to use the term "crisis" instead of "eruption" to describe period characterized by volcanic activity with intensity higher than the "ordinary" strombolian activity. The term "crisis" is more appropriate in the case of Stromboli because it has civil protection implications. A single crisis comprises different phenomena, such as higher-intensity strombolian explosions, lava overflows, major explosions, flank effusions and/or paroxysmal explosions. The large number of crises characterized by higher-intensity volcanic activity that occurred at Stromboli since the 2002–03 crisis has offered a unique opportunity to improve our understanding of how the volcano works. This study is an attempt to elaborate the 10-years-long GBInSAR time series in order to evaluate flank dynamics (and in particular the occurrence of intrusion-related landslides) and the occurrence of higher-intensity volcanic activity at Stromboli, providing an operative tool to mitigate their effects.

2. Geological and volcanological setting

2.1. Geological outlines

The 916 m-high Stromboli Island is the emerged portion of a ~3000 m-high volcano located in the north-eastern tip of the Aeolian Archipelago, in the southern Tyrrhenian Sea (Fig. 1a). The rock composition varies between basaltic andesite, shoshonite and latite-trachyte (e.g. Hornig-Kjarsgaard et al., 1993), with the oldest exposed products dated approximately 100 ka (Gillot and Keller, 1993).

Based on the presence of structural unconformities and changes in rock composition, the volcanic sequence of the subaerial cone has been subdivided into five periods of activity (Rosi, 1980; Hornig-Kjarsgaard et al., 1993; Keller et al., 1993; Tibaldi et al., 2008; Calvari et al., 2011c; Vezzoli et al., 2014): 1) Paleostromboli I (Cavoni synthem; 85–64 ka); 2) Paleostromboli II and Paleostromboli III (Gramigna synthem; 64–26 ka); 3) Lower, Middle and Upper Vancori (Frontone and Vancori synthems; 26–13 ka); 4) Neostromboli (Fossetta synthem; 13–6 ka); 5) Recent Stromboli (Pizzo, Fili di Baraona and Sciara synthems; 6 ka-present day activity).

Stromboli volcano was affected by three caldera collapses and at least five sector collapse events, which were followed by

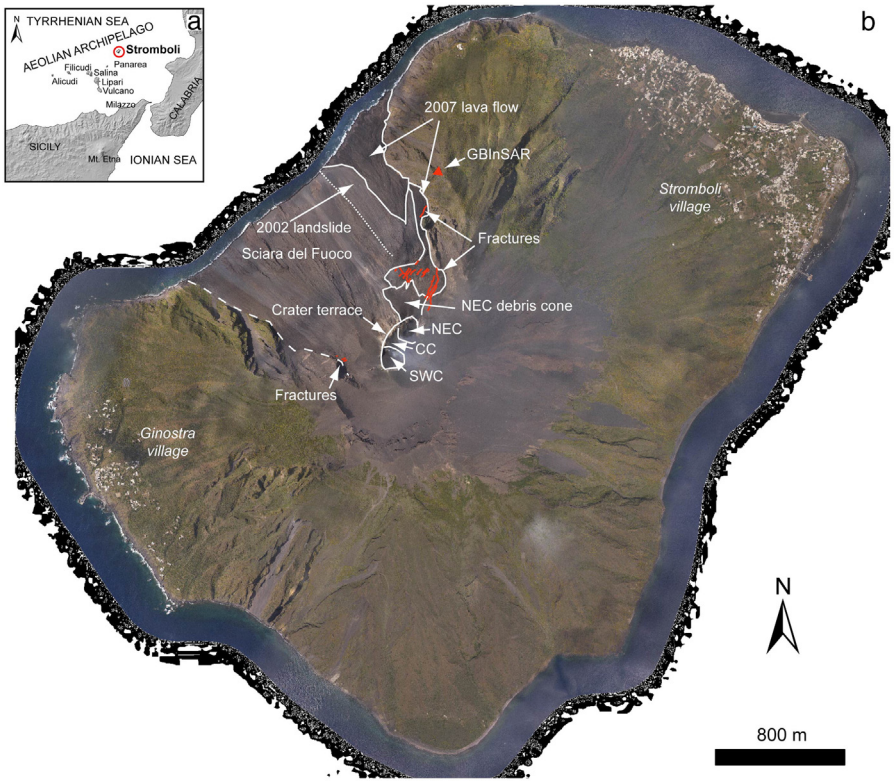

Fig. 1. a) Geographic location and b) setting of Stromboli Island after the 2007 crisis, highlighting the main structural features of the Sciara del Fuoco and summit crater area. National Civil Protection Department (DPC) is acknowledged for providing the ortophoto.

reorganizations of the eruptive centres (Tibaldi, 2001). The oldest sector collapse affected the SE flank of the edifice and occurred between 35 ka and 26 ka (Tibaldi et al., 2008; Romagnoli et al., 2009). Since 13 ka, lateral collapses only developed on the NW side of the volcano, forming a nested horseshoe-shaped scar (Fig. 1b and c) called the Sciara del Fuoco depression (Tibaldi, 2001). During the Holocene, (Neostromboli period – Fossetta synthem), volcanic activity was mainly concentrated in the NW part of the volcano, producing thin lava flows erupted either from central vents, or from ephemeral vents and eruptive fissures in the previously NW laterally collapsed area. The NW sector of the Neostromboli edifice failed during a lateral collapse and the formed lateral depression was nested within the previous ones (Tibaldi, 2003; Apuani et al., 2005a,b; Tibaldi et al., 2008). This collapse event occurred 5.6 ± 3.3 ka (Tibaldi, 2001), and produced a massive landslide (0.73 ± 0.22 km^3) and it has been related to a large explosive eruption (Secche di Lazzaro pyroclastic succession; Bertagnini and Landi, 1996; Tibaldi, 2001; Di Roberto et al., 2010). Another large landslide, that has cut a lava overflow in the NW sector of the Sciara del Fuoco, most likely occurred in the XIV century (Arrighi et al., 2004; Speranza et al., 2008) and produced a submarine turbidite deposit (Di Roberto et al., 2010). The most recent landslide of notable importance (25–30 × 10^6 m^3, Marani et al., 2009) is related to the 2002–03 crisis. It occurred the 30 December 2002 (Bonaccorso et al., 2003; Baldi et al., 2008) and caused two tsunami sequences with a max run-up of 6–7 m at Stromboli village (Tinti et al., 2006). The landslide was caused by the injection of a lateral intrusion (Neri et al., 2008) and observations indicated that a relatively deep-seated scar (≈200 m) affected the northern side of the Sciara del Fuoco (Baldi et al., 2008). Significant deformations were observed during the 30 December 2002 event but the displaced mass did not collapse as a whole but it fragmented into several "blocks". The largest block collapsed producing the second tsunami wave, while the first tsunami was generated by a submarine slide (Chiocci et al., 2008; Boldini et al., 2009). Tsunamis also occurred in recent times as in 1879, 1916, 1919, 1930, 1944 and 1954 (Barberi et al., 1993; Rosi et al., 2013). In all these events, the chronicles reported an initial withdrawal of the sea and therefore it is likely that all the known events were triggered by submarine landslides of the SdF (Rosi et al., 2013 and references therein). In the chronicles there is no mention of any landslides along the SdF prior to 2002 and thus tsunamis were more likely related to the destabilization of the submarine portion of the SdF by the accumulation of materials derived from the sub aerial counterpart, especially during the paroxysmal explosions (Barberi et al., 1993).

During the last crisis related to a flank eruption (February–April 2007), another flank effusion occurred (Barberi et al., 2009). The opening of the effusive vents at the base of the NE crater and in the SdF area produced small landslides, but tsunamis were not detected (Barberi et al., 2009). This lack of large instability phenomena has been related to the lower magmatic pressures that developed at the tip of the intrusion (Neri et al., 2008).

The SdF depression is filled with volcaniclastic deposits and lavas emitted by the central craters and from ephemeral vents within it (Calvari et al., 2005). Slope instability phenomena can be of several types (Tommasi et al., 2005; Falsaperla et al., 2008; Intrieri et al., 2013): 1) giant deep-seated gravitational slope deformations as those recognized in the past history of Stromboli (volumes >10^6 m^3); 2) shallower, large and more frequent landslides, such as the one which occurred in late December 2002, involving loose deposits and rock masses (volumes ≈ 10^6 m^3); 3) very superficial landslides, involving loose or weakly consolidated deposits (volumes ≈ 10^5 m^3).

The transition between the Neostromboli and the Recent Stromboli cycle (ca. 5,000 years b.p.; Gillot and Keller, 1993; Di Roberto et al., 2010) was associated with the collapse of the Fossetta crater (Finizola et al., 2003). After that, a pyroclastic cone was built by explosive activity that emplaced alternating ash tuff layers and scoriaceous spatters. During this activity, a large circular crater about 350 m in diameter, the Pizzo crater, formed (Fig. 1b). Then, a complex of nested craters (Fossa

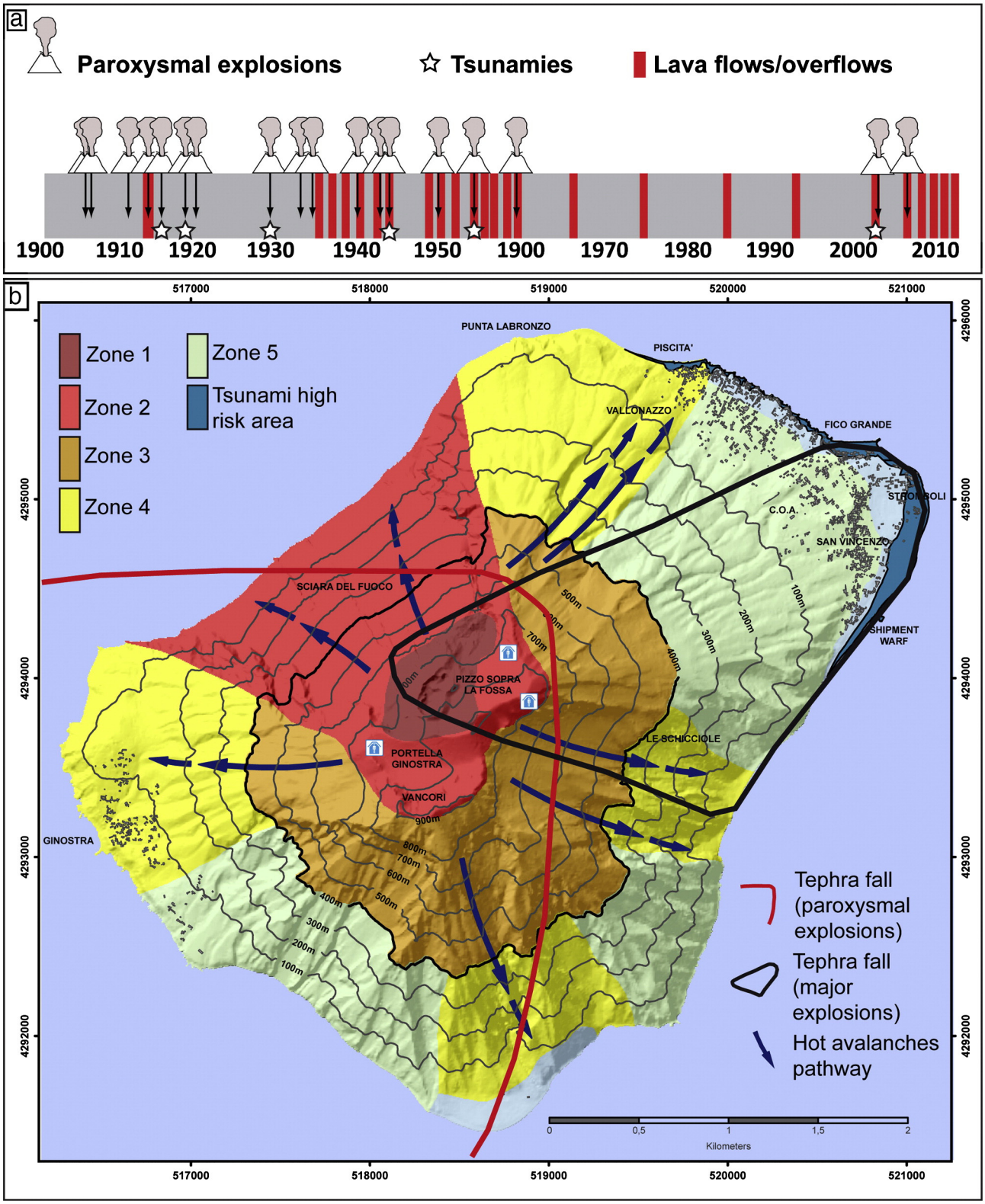

Fig. 2. a) Volcanic activity at Stromboli volcano since 1900 (data from Barberi et al., 1993; Rosi et al., 2013); b) volcanic and tsunami hazard map at Stromboli Island (modified after Nave et al., 2010 and Rosi et al., 2013). Zone 1: it is the zone around the active craters. It is exposed to hazard at any time, because of the possibility of a sudden blast from an obstructed (reopened) vent. The area is frequently affected by fallout of blocks and bombs (large, hot or cold rock fragments) ejected during the normal explosive activity. Zone 2: This zone may be affected by ballistic ejecta during major explosions (and paroxysms). Toxic gases may reach here troublesome concentrations. The Sciara del Fuoco, exposed to tephra (ash and rock fragments) fallout, landslide and lava flow hazard, is included in this zone. Zone 3: it is a zone intermediate between the one exposed to risk for major explosions (Zone 2) and the much larger one that may be affected during paroxysms (Zone 4). Its width varies as a function of the energy of explosive events. From the historical data the lower limit can be reasonably placed at the elevation of 400 m. During major explosions, this zone is affected by fallout of ash, lithic ejecta and incandescent lava fragments, with development of fires. Dangerous accumulation of ash, as well as ash avalanches may occur on the steep slopes. Zone 4: it is the zone affected by tephra (ash and rock fragments) fallout in case of a large, paroxysmal eruption. Ash showers, episodically accompanied by the fall of large blocks or bombs (hot or cold rock fragments), with fires and roof collapses, are the expected hazards. Breathing may be difficult in case of wind-driven dense ash and gas laden steam clouds. Zone 5: it is the safest zone of Stromboli where only minor ash showers may occur. The low coasts may be affected by small tsunamis. Tsunami high risk area: area to be left immediately during threat of a tsunami, such as when the sirens sound or the sea retreats (Nave et al., 2010).

crater, 1930 crater, 1954 crater, 2002–03 crater; Finizola et al., 2003) later opened within the Pizzo crater. It comprises the Large and the Small Fossa craters, respectively about 280 and 150 m in diameter (Finizola et al., 2003). The presently summit active cone is a composite pyroclastic cone, elongated NE-SW, where three main craters can be recognized (SW, central, and NE). Finizola et al. (2002), revealed the presence of a continuous impermeable layer at a constant depth (≈200 m), likely represented by crushed material rich in hydrated and altered minerals such as clay, that could represent the sliding plane of the type 2 SdF landslides.

2.2. Volcanic activity at Stromboli volcano

The 'ordinary' Strombolian activity consists of passive magma degassing alternated to brief (a few to few tens of s), 100- to 200-m high scoria-rich jets produced by explosions of variable energy every 10–20 min (Patrick et al., 2007; Andronico et al., 2008; Taddeucci et al., 2012), classified as having a Volcanic Explosive Index (VEI; Newhall and Self, 1982) within the −7/−3 range (Houghton et al., 2013).

This activity is occasionally interrupted by explosive events with higher intensity than the ordinary activity at Stromboli (Barberi et al., 1993; Rosi et al., 2013), defined as 'paroxysmal' (VEI = 0/1) and 'major' (VEI = −2/−1; Fig. 3) explosions, considered as the two higher-intensity 'variations on the Strombolian theme' (Rosi et al., 2000; Hougthon and Gonnermann, 2008; Del Bello et al., 2012). Ordinary activity is fed by high-porphyritic (HP), volatile-poor magma, while during paroxysmal and major explosions low-porphyritic (LP), volatile-rich magma is ejected (Landi et al., 2008; Bertagnini et al., 2011; La Felice and Landi, 2011). Even though they have very similar characteristics in the hand specimen, LP clasts of major and paroxysmal explosion show different textural features (Pioli et al., 2014). The LP clasts erupted during the paroxysmal explosion represent magma batches derived from the deeper reservoir beneath Stromboli (max. 4 km), while LP magma erupted during the major explosions represents the feeding zone of the HP reservoir, which is continuously hybridized by regular arrivals of the deep-derived magmas (Pioli et al., 2014).

The ordinary activity is produced once a gas slug – a discrete volume of gas rising in the conduit system at a relatively higher velocity with respect to the surrounding mafic magma – reaches the cooled upper surface of a magma column causing its raising, up-doming and ultimately the explosive release of gas that is accompanied by the ejection of magma clots (Blackburn et al., 1976; Vergniolle and Brandeis, 1996; Parfitt, 2004; Hougthon and Gonnermann, 2008). The bursting of overpressured slugs has been invoked as a general mechanism to explain the entire spectrum of eruptive dynamics at Stromboli (Allard, 2010; Del Bello et al., 2012). Ordinary activity is associated with a relatively shallow origin of the gas source (800–2700 m Burton et al., 2007a), while major and paroxysmal explosions are related to larger gas slugs that are in equilibrium with the magma at depth greater than 4 km below the crater terrace (Allard, 2010; Métrich et al., 2010; Aiuppa et al., 2011). These may be the depth of slug formations, even if recent studies (Rivalta et al., 2013) revealed the possibility that the delay in vesiculation can occur in mafic, low-porphyritic magmas, altering the actual depth of slug formation.

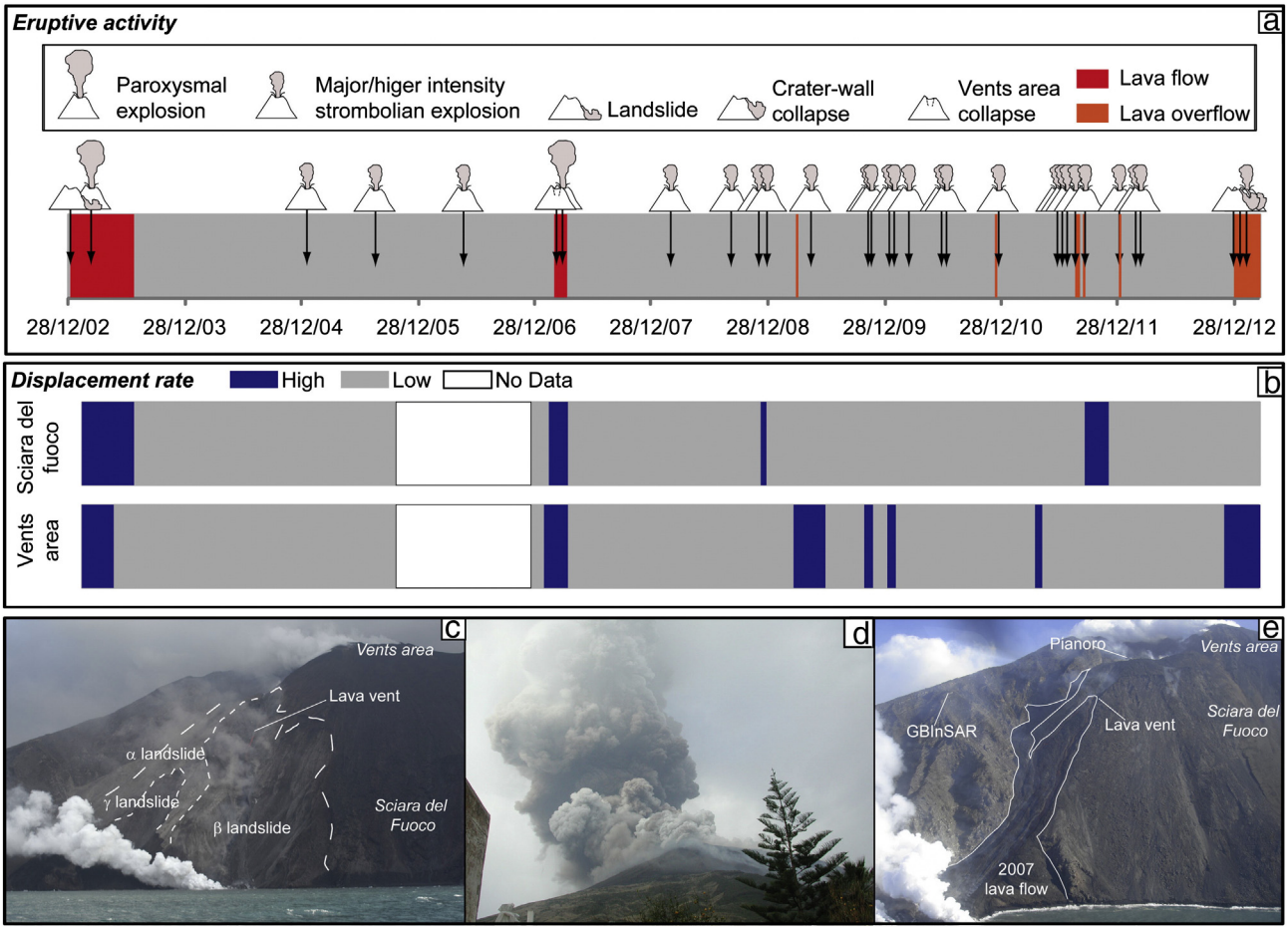

Fig. 3. Diagrammatic representation of a) eruptive activity and b) ground deformation at Stromboli in the period December 2002–May 2013; c) Sciara del Fuoco area after the 30 December 2002 tsunamigenic landslides; d) 5 April 2003 paroxysm; e) lava flow in the Sciara del Fuoco area during the 2007 flank eruption crisis.

Paroxysmal explosions are often associated with flank effusive eruptions (Calvari et al., 2011b), which are almost anticipated by major changes in the activity of the volcano (Lautze and Houghton, 2005; Rosi et al., 2006; Pistolesi et al., 2008, 2011; Andronico et al., 2013) and hence their occurrence can be estimated (Casagli et al., 2009; Calvari et al., 2011a; Inguaggiato et al., 2011). The 5 April 2003 and the 15 March 2007 paroxysmal explosions took place when a threshold lava volume (~4.0×10^6 m^3) was erupted, implying that paroxysmal events can occur after the start of an apparently gentle effusive eruption (Calvari et al., 2011b).

Only a few precursors have been revealed for major explosions (Aiuppa et al., 2011; Di Traglia et al., 2013). In general, major explosions are clustered in a relatively short time period (1–2 months) of 'anomalous' activity during which the 'ordinary' Strombolian activity is characterized by more frequent events (>5 events per hour, Andronico et al., 2008; Taddeucci et al., 2013), by formation of a cool crust in one of the craters (Calvari et al., 2011a; Gurioli et al., 2014), by high CO_2 soil and plume fluxes (>1000 tons per day, Aiuppa et al., 2011), by high displacement rate in the crater area (Di Traglia et al., 2013, 2014a,b) and they are generally associated with the emission of lava from the summit craters (Rosi et al., 2013).

3. Materials and methods: the GBInSAR monitoring system at Stromboli volcano

The GBInSAR consists of a ground-based interferometer (Fig. 4a, b) producing 1 SAR image every 11 min of the NE flank of the crater area and the upper part of the SdF. Radar images are obtained through sampling techniques, so frequency and spatial steps have to be selected in order to avoid ambiguity in range and cross-range (Antonello et al., 2004). The system is able to measure line-of-sight (LoS) ground displacement in the time interval between two acquisitions and the displacement is calculated from the phase difference between the back-scattered signals received at different times, through the cross-correlation between two SAR images. Interferometric analysis allows us to derive the displacement field of the observed portion of the SdF and of the crater area in the elapsed time. Negative and positive values of displacement indicate, respectively, a movement towards or away from the sensor. Since the GBInSAR is located in a stable area north of the SdF, and its LoS allows us to detect the N-S components of the movements in all direction (Fig. 4c); negative displacement may represent inflation of the crater area of the volcano or inflation and sliding of the SdF, while positive displacement may represent deflation of the crater area (Casagli et al., 2009). Range and cross-range resolution are on average 2 m × 2 m, with a measurement precision referred to the displacement of less than 1 mm (Casagli et al., 2009). The displacement rate is the result of the mathematical division between the displacement measured in an interferogram (referred to the difference between two SAR images) and the elapsed time between the two images. The key concept of the GBInSAR data analysis is the elapsed time between the two SAR images used to create interferograms, allowing the identification of very low displacement rates (0.01–0.001 mm/h) related to the creep of the northern sector of the SdF (Intrieri et al., 2013; Nolesini et al., 2013) or very fast displacement rates (up to 300 mm/h) associated with effusive vent opening (Casagli et al., 2009). The capability of InSAR to detect ground displacement depends on the persistence of phase coherence over appropriate time intervals (Lu et al., 2002). Loss in coherence mainly depends on chaotic ground movements (Antonello et al., 2004), e.g. grain avalanches. A coherence mask (threshold = 0.8) is set to mask the noisy areas of the interferogram (Luzi et al., 2010). The phase values can be affected by ambiguity (unwrapped phase) but, due to the short elapsed time (11 min) between two subsequent measurements on Stromboli volcano, the interferometric displacements are usually smaller than half wavelength and unwrapping procedures (as described by Ghiglia and Romero, 1994) are not necessary.

The data presented in this review cover the entire 10 years of monitoring even if the system has undergone a few stops due to malfunctions and maintenance (2005–2006: Fig. 3).

4. Monitored sectors

Throughout the first months of data recording, it was possible to define two zones with different movements: the SdF and the NE crater area. After the 2007 crisis, the analysis of the displacements has been performed by dividing the part of the volcano monitored by the GBInSAR into 5 regions (Fig. 1): 1) the crater rim of the NE cone; 2) the flanks of the crater area; 3) the slope at the base of the NE pyroclastic cone; 4) the portion of the SdF within the 2002 tsunamigenic landslide (α landslide; Tommasi et al., 2005); 5) a small portion of the SdF outside of the 2002 tsunamigenic landslide.

Sector 1 is a small area at 750 m a.s.l., corresponding to the rim of the NE crater area, characterized by low coherence of the GBInSAR signal due to the fast and continuous remobilization of the products ejected by the crater. High displacement rates have been detected in short temporal baseline interferograms (11 minutes–1 hour). The geometry of the displacement reveals the presence of unstable materials on the

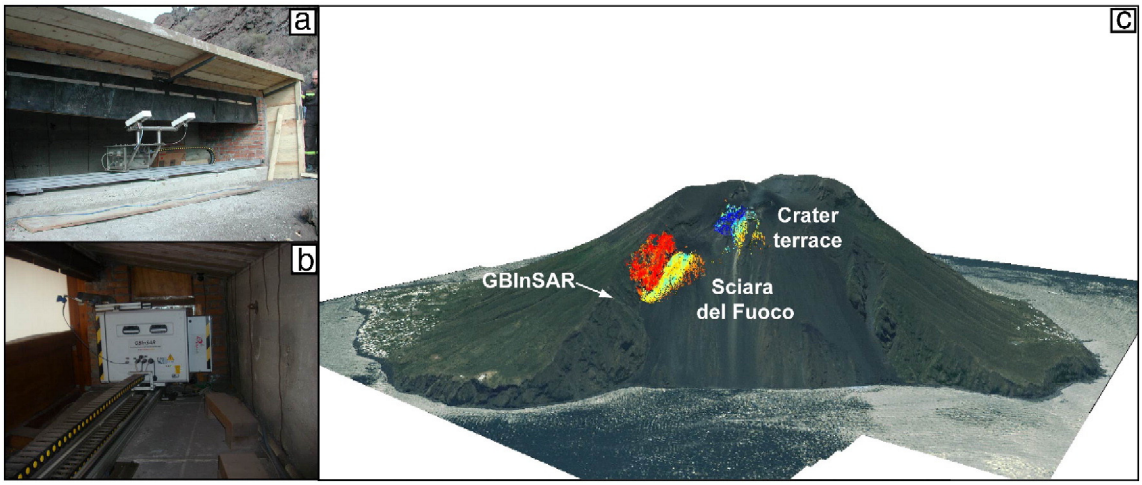

Fig. 4. The GBInSAR system in the a) 2003 and b) 2009; c) GBInSAR cumulative displacement map (2010–2013) highlighting sensor the Field of View (FOV).

outer slope downhill the rim of the NE crater, with peaks in the displacement rate up to 30 mm/h.

Sector 2 corresponds to the external flank of the crater terrace and it is positioned on the Recent Stromboli deposits (Keller et al., 1993) mainly characterized by scoria products and thin lava flows (Tibaldi et al., 2008). Sector 2 is characterized by two types of displacements: i) long-lived movements, which have maximum displacement at the boundary between sector 2 and 3 (Fig. 5), and ii) short-living movements, interpreted as syn-explosive deformations linked to higher-intensity explosions (Tarchi et al., 2008; Di Traglia et al., 2013).

Sector 3 corresponds to the slope at the base of the NE pyroclastic cone, just below sector 1. The location of the maximum displacements in sector 3 changed with time, affecting areas at different elevation (Fig. 5), between 700 m and 600 m a.s.l..

Sector 4 corresponds to the upper part of the 2002 landslide (α landslide in Tommasi et al., 2005), which occurred on the 30 December 2002 at the beginning of the 2002–2003 crisis (Intrieri et al., 2013). This sector is characterized by a scar produced by a retrogressive landslide that occurred soon after the eccentric vent opening at 400 m a.s.l. during the 2007 crisis (Casagli et al., 2009), just below sector 4. This scar is prone to continuous erosion, resulting in further deepening, and by sporadic lava accumulations produced by lava overflows (Di Traglia et al., 2013). On the other side, sector 5 comprises an area of the SdF external to the α landslide that was subject to a large accumulation of recent lava flows (1985; 2002–2003 and 2007; Intrieri et al., 2013), with an average thickness of 20–30 m for each flow (Baldi et al., 2008; Giordano and Porreca, 2009; Marsella et al., 2012).

5. The 2002–2013 eruptive crises

5.1. 2002–03 crisis

The 2002–03 crisis started the 28 December 2002, after an intensification of the volcanic activity started on November 2002 (Lautze and Houghton, 2007), with the opening of a NE-SW trending eruptive fissure that extended from the NE vents, at an elevation of about 750 m a.s.l., down to 600 m elevation (Table 1, Fig. 6b). On the morning of the 30 December 2002, a huge landslide started on the Sciara del Fuoco, moving about 25–30 million m^3 of stratified deposits (Marani et al., 2009). The landslide, described in detail by Tommasi et al. (2005), was developed in 4 different bodies, three affecting the sub aerial portion and one the submerged. The collapse of the submerged and part of the sub aerial slope triggered two tsunamis separated by 10 minutes (Tinti et al., 2005) causing damages all along the island coast.

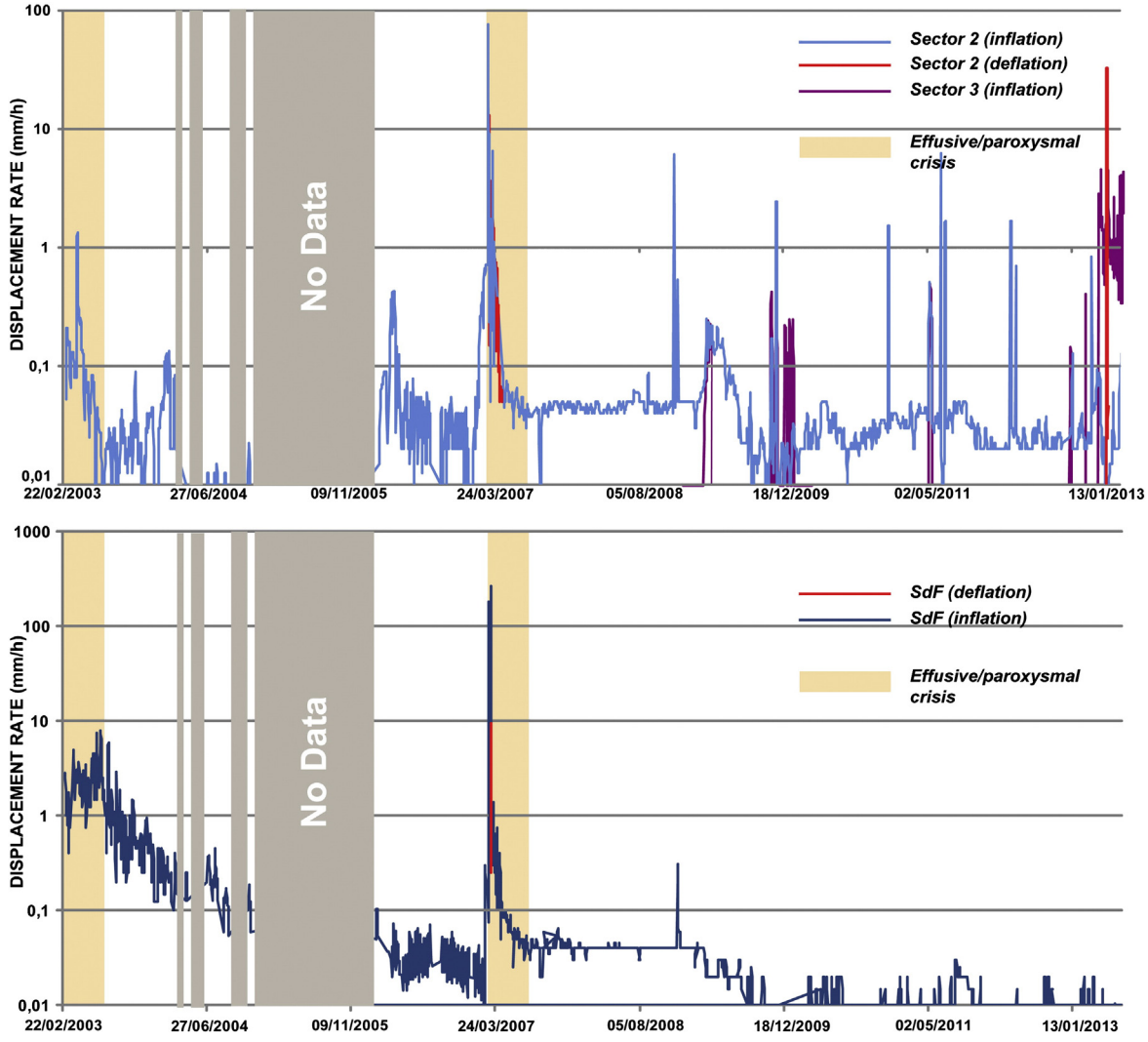

Fig. 5. Displacements recorded by the GBInSAR system since January 2003 in the a) crater area and b) Sciara del Fuoco.

Table 1
Summary of significant eruptive events at Stromboli between December 2002 and May 2013 (modified from Rosi et al., 2013). References column: 1) Calvari et al., 2005; 2) Antonello et al., 2004; 3) Rosi et al., 2006; 4) Andronico et al., 2008; 5) Aiuppa et al., 2009: 6) Casagli et al., 2009; 7) Aiuppa et al., 2010; 8) Pistolesi et al., 2011; 9) D'Oriano et al., 2011; 10) Calvari et al., 2012; 11) Carbone et al., 2012; 12) Madonia and Fiordilino, 2013; 13) Intrieri et al., 2013; 14) Aiuppa et al., 2011; 15) Di Traglia et al., 2013; 16) Nolesini et al., 2013; 17) Di Traglia et al., 2014a.

Date	Type of Activity	Note	GBInSAR data	References
December 2002–July 2003	Effusive – paroxysm	Eruption onset: 28 December 2002; tsunamogenic landslide: 30 December 2002; eruption end: 21–22 July 2003; paroxysmal explosion 5 April 2003.	The Sciara del Fuoco exhibits a displacements deriving by the superimposition: 1. lava flows which move at a high speed rate; 2. gravitational sliding of the volcanoclastic materials on the 30 December 2002 landlside slip surface; 3. gravitational slow viscous flow of cooling lava flows. Strong syn-paroxysm deformations.	1, 2, 3
June 2004–January 2005	Higher-intensity explosions	Explosions characterized by higher energy than the normal explosive activity, mainly in terms of column height and dispersal of products.	No detected displacements.	4
15 December 2006	Major explosion	High CO_2/SO_2 ratios (December 2006).	Increase in displacement rate in the vents area since late November 2006.	5
February–April 2007	Effusive – paroxysm	Eruption onset: 27 February 2007; eruption end: 12 April 2007; paroxysmal explosion 15 March 2007. Low temperature fumaroles increase temperature: 10 February 2007. Persistence of pre-effusive anomalously high CO_2/SO_2 ratio (peak 13 February 2007).	Continuous acceleration on the crater area since 10 January 2007. Increase in the displacement rate in the SdF since 15 February 2007.	6, 7, 8
7 September 2008	Major explosion	Anticipated by one week of high LP magma in the erupted ash, gravity anomaly, low temperature fumaroles higher temperature.	Syn-explosions displacement.	9, 10, 11, 12
6–17 December 2008	Major explosions		Syn-explosions displacement. Increase in the SdF displacement rate between 12–16 December 2008.	13
May 2009	Major explosions – overflows	Higher-intensity activity in April–May and 2009. Several intracrater lava overflows. Major explosions: 3 May 2009	High displacement rate in sector 3 before (~1 month) explosion. Slight increase in displacement rate in sector 2.	14,15
November 2009–December 2010	Major explosions – overflows	Four major explosions. High CO_2 soil flux, low temperature fumaroles higher temperature.	High displacement rate in sector 3 before (~5 five days) explosions. Slight increase in displacement rate in sector 2.	14,15
June–September 2011	Major explosions – overflows	Seven major explosions, two overflows. High CO_2 soil flux, low temperature fumaroles higher temperature.	High displacement rate in sector 3 before (~1 month) explosion. Slight increase in displacement rate in sector 2. Increase SdF displacement rate (August–October 2011).	12, 14,16
December 2012–June 2013	Major explosions – overflows	Several lava overflows, major Strombolian explosions, crater-wall collapses pyroclastic density currents and intense spatter activity.	High displacement rate in sector 2 and 3.	17

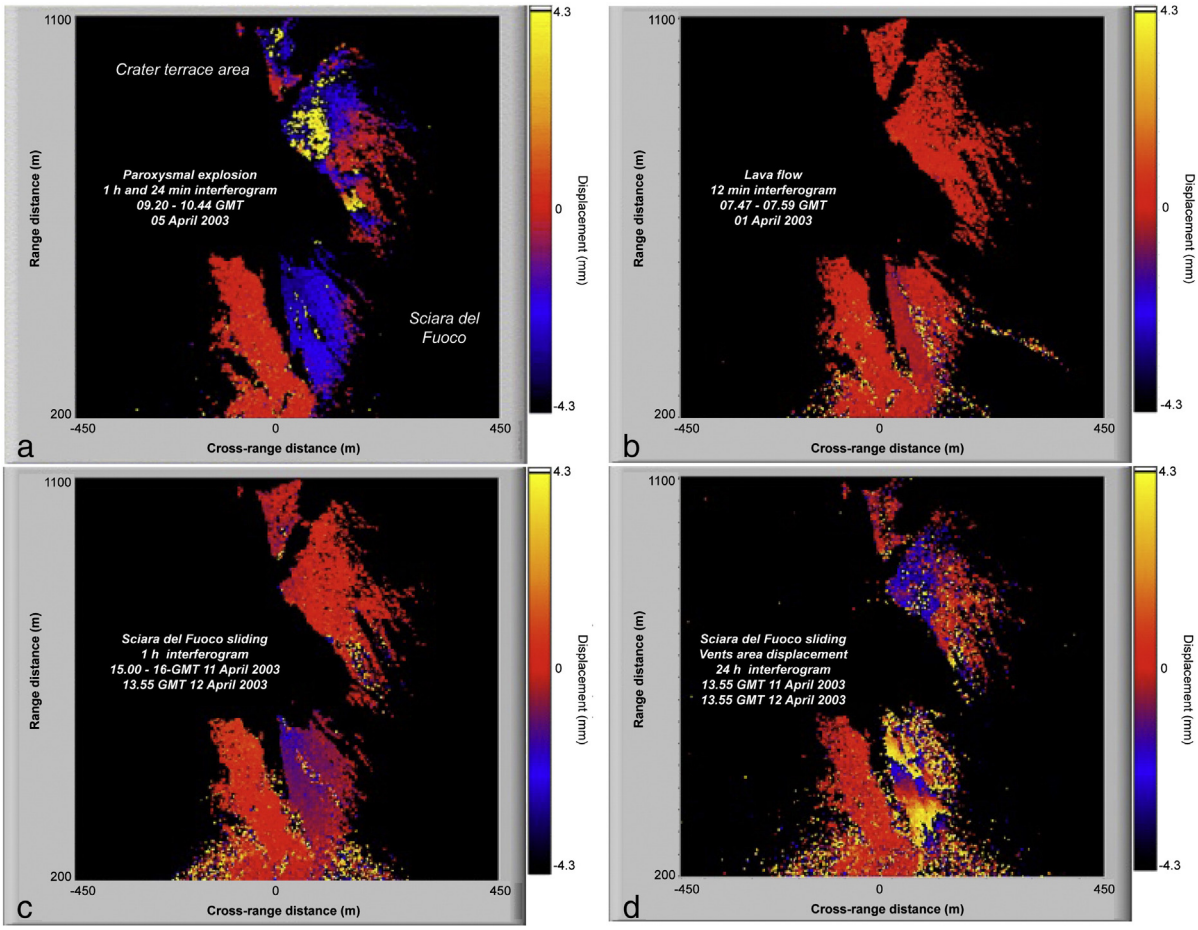

Fig. 6. Interferograms during the 2002–03 crisis. a) Interferogram (1 hour and 24 minutes time interval) during the 5 April 2003 paroxysm; b) interferogram (11 minutes time interval) during the 2003 lava flow; c) interferogram (1 hour time interval) and d) interferogram (24 hours time interval) during 2003 crisis showing the sliding of the Sciara del Fuoco.

In the crater area, the average velocity detected by the GBInSAR (Fig. 5a) during February-April 2003 was about 0.13 mm/h, as opposed to very slow displacement rates (0.02–0.03 mm/h) recorded during the rest of the crisis (until July 2003). The explosion of 5 April 2003 caused a fast increase in velocity bolting from 0.03 mm/h to 3 mm/h (Fig. 6a). The return to normal values happened two months later (Antonello et al., 2004; Tarchi et al., 2008).

The displacement rate in the SdF (Fig. 5b) was about 3 mm/h, with peak values varying from 4–5 mm/h (21–26 March 2003) to 10 mm/h (22 July 2003) (Fig. 6c, d). Since July 2003, after the end of the effusive phase, a progressive diminution of the displacement rates was recorded (0.1–0.3 mm/h).

5.2. 2004–2006 crises

Two crises characterized by anomalous volcanic activity occurred between the 2002–03 and the 2007 crises (Table 1): June 2004–January 2005 and December 2006. These crises were characterized by the increase of the magma level within the conduit, by the increase in the average number of explosions per day and by the occurrence of higher-intensity strombolian explosions (Andronico et al., 2008; Coppola et al., 2012). The GBInSAR system did not work between late November 2005 and November 2006. After the system was reactivated, GBInSAR detected an increase in the displacement rate since November 2006, before the 16 December 2006 major explosion (Fig. 5).

5.3. 2007 crisis

The 2007 Stromboli crisis was characterized by an effusive eruption punctuated by a paroxysmal explosion that occurred the 15 March 2007 (Barberi et al., 2009; Pistolesi et al., 2011). The crisis started with the breaching of the NE flank of the crater area which occurred on 27 February 2007, anticipating the opening of the first ephemeral vent at 650 m a.s.l. at the base of the NE crater area (Table 1 and Fig. 7a; Barberi et al., 2009; Casagli et al., 2009). In the afternoon of the same day an increase of the seismic activity was recorded and a second ephemeral vent opened at 400 m a.s.l. within the SdF (Giordano and Porreca, 2009). A series of fractures were observed on the crater area since the early March, then a collapse of the entire crater area occurred (Casagli et al., 2009; Giordano and Porreca, 2009). This collapse generated a partial obstruction of the conduit that eventually caused the closure of the second ephemeral vent that re-opened on 9 March 2007. A paroxysmal explosion was registered on 15 March 2007 with a magnitude similar to the 5 April 2003 paroxysmal event (Calvari et al., 2010; Pistolesi et al., 2011; Bonaccorso et al., 2012; Andronico et al., 2013). The eruptive crisis ended on 2–3 April 2007 (Barberi et al., 2009).

Starting from 10 January 2007 a continuous increase of the displacement rate of the crater area had been recorded by the GBInSAR system (Fig. 5a). Values changed from 0.04 to 0.7 mm/h moving towards the sensor until the onset of the effusive eruption (27 February 2007). A series of concentric interferometric fringes were visible in the GBInSAR images on the upper part of the crater area (Fig. 7b). This increase in the displacement rate has been related to the inflation of the upper

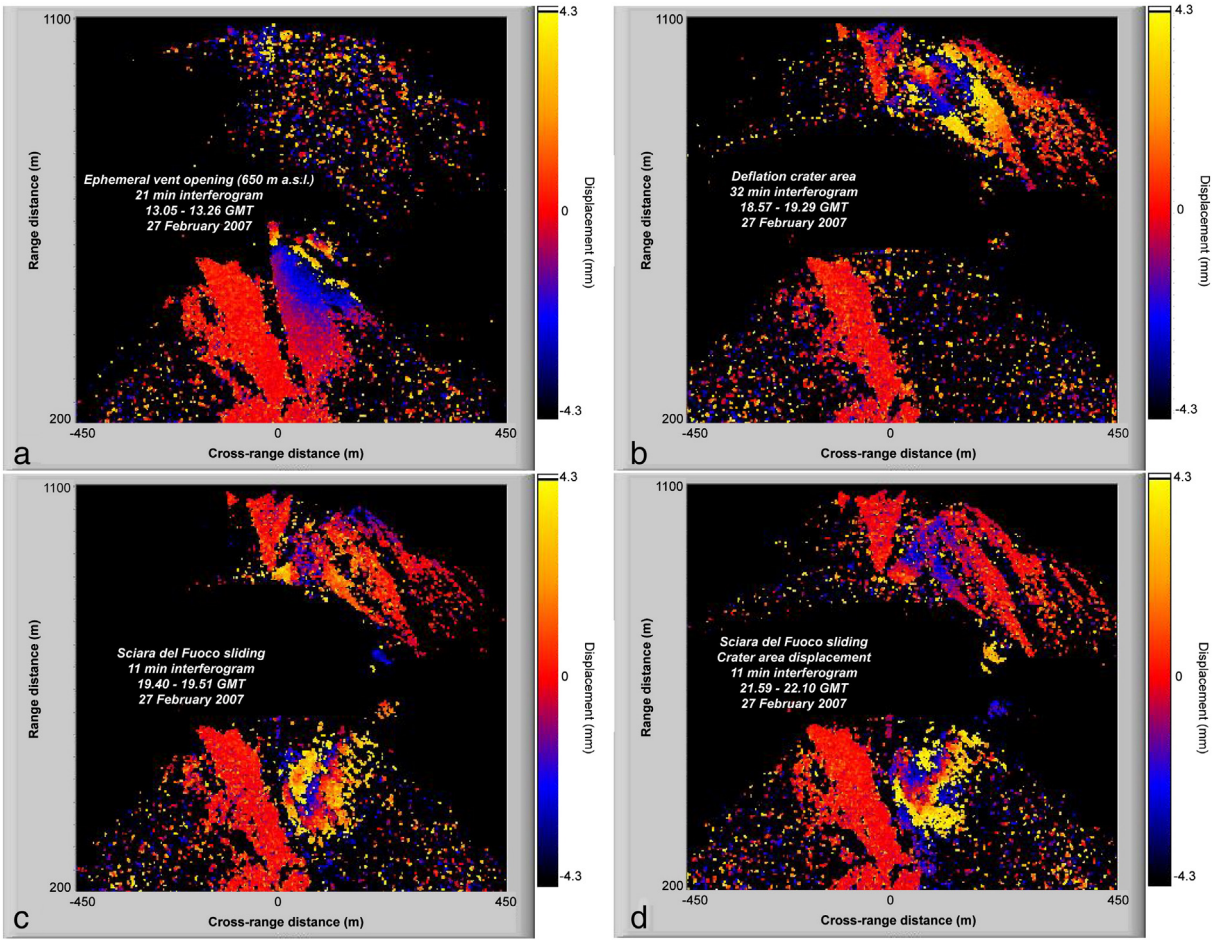

Fig. 7. Interferograms during the 2007 crisis. a) interferogram (21 minutes time interval) during the 27 February 2007 vent opening; b) interferogram (12 minutes time interval) during the inflation after 27 February 2007 vent opening; c) interferogram (11 minutes time interval) and d) interferogram (24 hours time interval) during 2003 crisis showing the sliding of the Sciara del Fuoco.

part of the volcanic edifice (Casagli et al., 2009). The base of the NE crater area, near to the collapsed Pianoro area (Fig. 7c), showed a displacement rate in the range of 10–12 mm/h. Between 27 February and 12 April 2007 the GBInSAR system was able to record, on the crater area, two cycles of displacements towards and backwards with respect to the sensor. In detail, the GBInSAR recorded inflation before the opening of each effusive vent and a deflation afterwards (from −1.5 mm/h to +6 mm/h on 27 February 2007, and from −0.5 mm/h to +7.0 mm/h on 15 March 2007; Fig. 5a). During the 15 March 2007 paroxysmal explosion, a rapid increase in the displacement rate was recorded in the crater area (7.0 mm/h; Fig. 7a; Casagli et al., 2009).

Since 15 February 2007, on the upper part of the SdF the GBInSAR recorded a sudden increase in the displacement rate from 0.02 to 0.25 mm/h, which was maintained until the eruptive crisis onset, on 27 February 2007, with displacement rate between 30 mm/h to 0.2 mm/h (Fig. 5b; Fig. 7c and d). Between 8 and 9 March 2007, the recorded displacement rate along the SdF increased again, from 1.5 mm/h to 5 mm/h. From 11:17 and 11:28 UTC of 9 March 2007, interferogram highlights a very high displacement rate (more than 300 mm/h), exceeding the capability of the correct phase unwrapping. This phenomenon has been recorded through the hours preceding the reopening of the ephemeral vent at 400 m a.s.l.. During the period 9–15 March 2007 the displacement rate in the SdF showed a constant value of about 0.5 mm/h (Fig. 5). No displacements were registered on the SdF during the 15 March 2007 paroxysmal explosion (Fig. 5).

5.4. 2008–2013 crises

Six crises characterized by anomalous volcanic activity occurred between 2008 and 2013 (Calvari et al., 2014): September 2008; December 2008; March–May 2009; November 2009–January 2010; June–September 2011; December 2012–May 2013 (Table 1).

During the September 2008 crisis, characterized by the occurrence of a major explosion (7 September 2008; Table 1; Calvari et al., 2011a) only a syn-explosive displacement of the crater area was recorded, while no precursory displacements were detected before the major explosion.

Throughout December 2008, characterized by the occurrence of two major explosions (6 and 17 December 2008; Table 1), in the crater area were recorded only syn-eruptive displacements during the major explosions (Fig. 5a), whereas a strong increase in the displacement rate was detected in the SdF (up to 0.5 mm/h) in the period 12–16 December 2008 (Fig. 5b).

Displacement rate in sector 3 increased progressively from 0.05 mm/h during early March to 0.35 mm/h on 27 March, just two days before the lava outflows from the summit crater area (Fig. 5). The displacements in sectors 2 and 3 (Fig. 5a) remained high (average about 0.11 mm/h) for the following two months with peaks on 3 April (0.27 mm/h) and 14 April 2009 (0.2 mm/h) and 3 May 2009 (0.25 mm/h, during a major explosion) and 22 May 2009 (0.23 mm/h). The 3 May 2009 explosion produced high-displacement rate in sector 2 at the time of the explosion (50.6 mm/h; Fig. 5a).

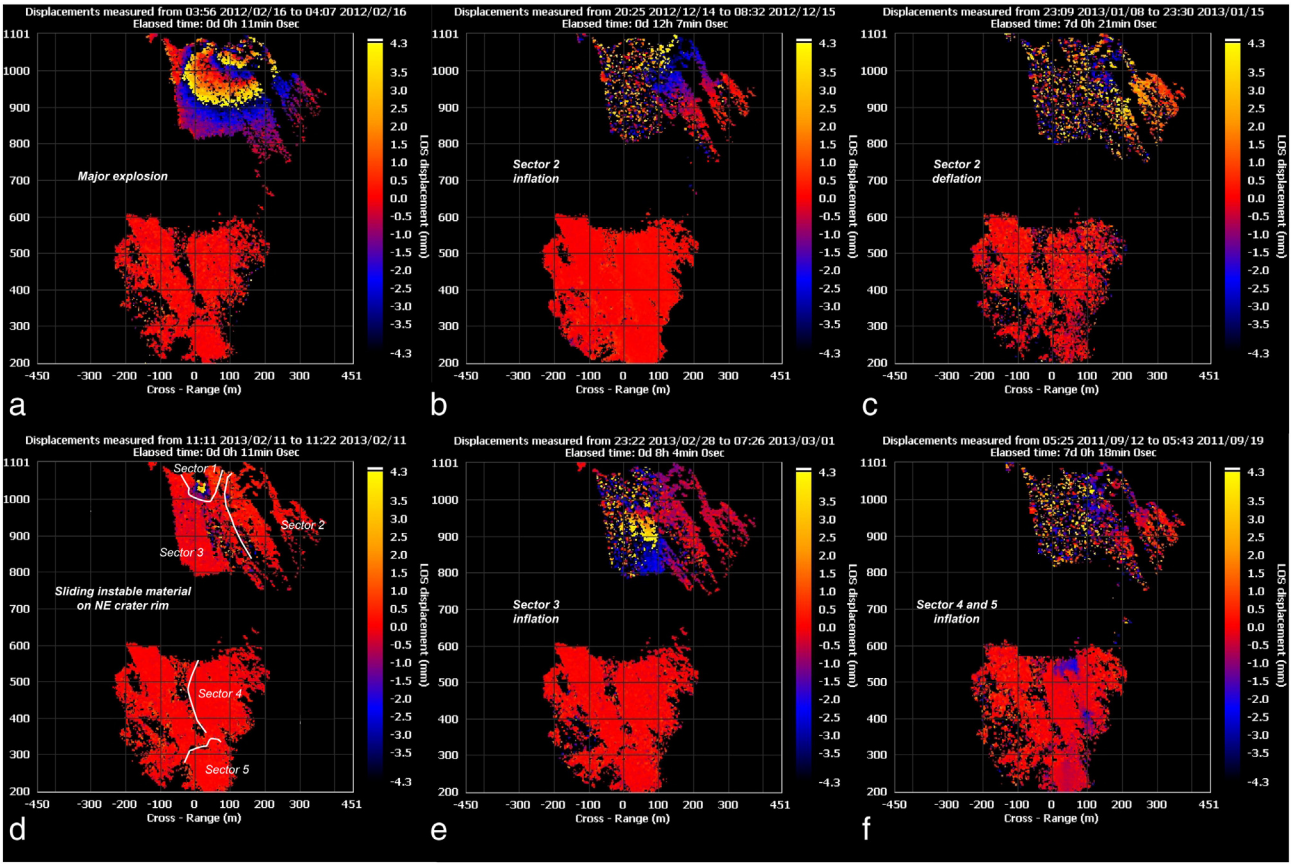

Fig. 8. Interferograms during the 2008–13 crises. a) interferogram (11 minutes time interval) during the 16 February 2012 major explosion; b) interferogram (12 hours time interval) showing inflation of the sector 2 before the 2012–13 crisis; c) interferogram (7 days time interval) showing deflation of the sector 2 before the 2012–13 crisis interferogram; d) interferogram (11 minutes time interval) showing the sliding of the materials on the rim of the NE crater; e) interferogram (8 hours time interval) showing inflation of sector 3 before the 2012–13; f) interferogram (7 days time interval) showing the inflation of the Sciara del Fuoco during the 2011 crisis.

Throughout the November 2009–January 2010 period an increase in the displacement rate was observed starting from 2 November 2009 (from 0.02 mm/h to 0.56 mm/h in sector 3) that ended with the explosion of 8 November 2009 (0.6 mm/h in sector 2). Analogous trends have been observed in the periods between 19 and 23 November 2009 (0.25–0.3 mm/h in sector 3), 20 and 28 December 2009 (0.25–0.29 mm/h in sector 3), 6 and 9 January 2010 (0.24–0.29 mm/h in sector 3) and finally, 16 and 20 January 2010 (0.2–0.3 mm/h in sector 3). During the 8 November 2009 and 24 November 2009 major explosions, the GBInSAR revealed a series of concentric fringes on the upper part of sector 2 on the 1-hour interferograms, showing a strong peak of displacement rate about 12.1 mm/h and 45.5 mm/h, respectively.

Before the June-September 2011 crisis, an increase in the displacement rate of sector 3 was recorded during May 2011. In the period 8–19 May 2011, on 4-hours and 8-hours interferograms, the bottom of sector 3 showed high coherence and a displacement rate up to 5.5 mm/h was recorded. The GBInSAR detected high displacement rate on sector 2 only during the 20 June 2011 (10.6 mm/h) and 5 July 2011 major explosions (6.5 mm/h), while displacement rate remained in the below 0.1 mm/h during all the crisis (Di Traglia et al., 2014b).

After the June-September 2011 crisis, isolated major explosions occurred on 16 February 2012, producing significant displacements in the crater sectors (Fig. 8a). A significant increase in the displacement rate was observed in sector 2 on 12-hour, 24-hour and 7-day interferograms, since the end of November 2012 (Fig. 8b). In detail, a strong increase in the values was observed from the end of November until the 22 December 2012 (from 0.01 to 0.12 mm/h); subsequently it decreased until 12 January 2013. Between 14 and 21 January 2013 the GBInSAR system registered a movement away from the sensor, coeval with a large overflow from the NE crater (Fig. 8c). Subsequently, between 1 and 6 February 2013 the GBInSAR registered displacements toward the sensor that increased again (0.08 mm/h). A similar trend was recorded between 27 February and 13 March 2013 (peak at 0.18 mm/h).

During this period, some crater collapse events were observed, sometimes associated with the increase in the displacement rate in sector 1 (Fig. 8d). Regarding sector 3, corresponding to the debris cone of the NE crater, a significant increase in displacement rate values was recorded on 24-hours interferograms since 18 December 2012 (Fig. 5a). The displacement rate in sector 3 increased (1.7 mm/h) and remained at high levels (more than 1 mm/h) in all the period late December 2012–early March 2013 (i.e. Fig. 8e), with some fluctuations (increase/decrease). Peaks in displacement rate have been recorded on 24 December 2012 (10.9 mm/h), 24 January 2013 (2 mm/h), 27 January 2013 (1.8 mm/h), 7 February 2013 (8.6 mm/h), 22 February 2013 (5.3 mm/h), 1 march 2013 (8.1 mm/h), 3 March 2013 (7.6 mm/h), 4 March 2013 (8.1 mm/h) and 10 March 2013 (10.6 mm/h).

While the deformations in the crater area were well differentiated on short time interval interferograms, the movements on the SdF were slower and needed an appropriate time interval to be detected (monthly-annual interferograms; Intrieri et al., 2013; Nolesini et al., 2013). An increase in the displacement rate on sector 4 and 5 was recognized (28-day interferograms) starting on 8 November 2009 (0.019 mm/h) and ending on 13 November 2009, with the maximum

displacement located in the upper zone of each sector. A similar displacement has been observed on the two SdF sectors between 19 and 23 February 2010 (0.02 mm/h), in the period between the 10 January 2010 and 12 March 2010 major explosions. Since 1 January until 21 April 2011, the displacement rate had strong variations up to 0.014 mm/h. After these periods, the displacement returned on very low values (<0.01 mm/h) for a long period of time (22 April 2011–24 September 2011). During this period, on 1–2 August 2011 a lava overflow spilled from the NE crater reached sector 4 causing shallow landslides (Nolesini et al., 2013). Increase in the displacement rate was recorded in the period September–October 2011 (Fig. 8f) with a maximum value of 0.5 mm/day, then the displacement rate decreased again and returned to very low values (<0.01 mm/h). All through the entire December 2012–June 2013 period, the monitoring system recorded very slow movements in both Sciara del Fuoco's sectors (0.001–0.003 mm/h).

6. Discussions

6.1. Slope instability of the Sciara del Fuoco

The analysis of the entire dataset of GBInSAR measurements allowed the assessment of the deformation field of the SdF area. In detail, the main displacements recognized can be related to different factors: 1) the inflation/deflation respectively immediately before and after each new opening of effusive vents; 2) the bulging of localized sectors of the SdF involved in the vent opening; 3) the gravitational sliding of the SdF infill; 4) the movement of lava flows.

The low displacement rate (0.001–0.01 mm/h) observed by the GBInSAR system along the SdF suggests creep behaviour of the volcaniclastic material filling the depression. Planar deep creep occurs on long slopes when the strata dip parallel to the slope and the rocks

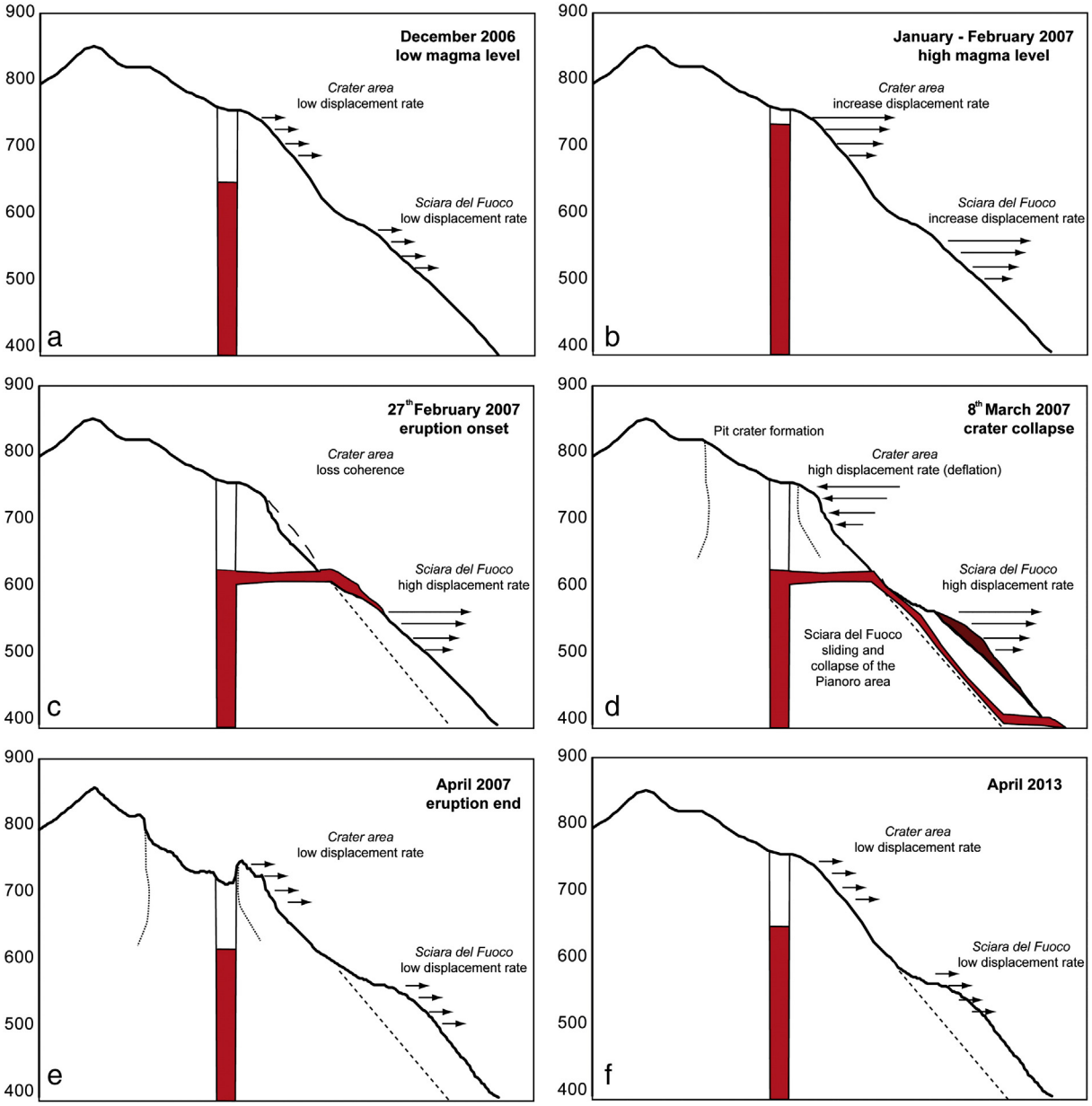

Fig. 9. Schematic reconstruction of the 2007 crisis. a) Pre-crisis situation (2006); b) unrest, showing the increase in the displacement rate in the crater area (sector 2), due to the increase in the magmastatic pressure in response to the rise of the magma level within the conduit; c) onset of the eruption, showing the decorrelation of the crater area and the increase in the displacement rate in the Sciara del Fuoco area; d) opening of the new vent within the Sciara del Fuoco due to magma migration from the 650 m a.s.l. to 400 m a.s.l. vents. This phenomenon was favoured by the segmenting and enlarging at the contact between the 2002–2003 lava which form the Pianoro and the 30 December 2002 landslide basal surface (Giordano and Porreca, 2009; Intrieri et al., 2013). The magma downward motion from the conduit towards the Sciara del Fuoco caused the crater area deflation ad subsequent collapse; e) and f) after the crises the displacement rate returned at pre-2007 values.

have different rheological characteristics (Ter-Stepanian, 1966). One of the possible mechanisms could be the sliding of lava on volcaniclastic products at many planar discontinuities, which has been observed by Boldini et al. (2009). Such mechanism is consistent with the pattern of the displacement maps recorded by the GBInSAR, as described by Intrieri et al. (2013). The seawards motions of the SdF can also occur based only on the force of gravity, without coeval magma intrusion (Tibaldi et al., 2009; Nolesini et al., 2013). After a period of creep movements, sheet intrusion can occur during a stage of increasing magma overpressure, relieving the extensional strain accumulated during the previous slip (Tibaldi et al., 2009). Slopes subjected to creep are prone to failure because the slow motion may reduce strength at shear zones (Voight and Elsworth, 1997; Hurlimann et al., 2001).

GBInSAR data, together with field observations carried out after the onset of the 2007 crisis (Casagli et al., 2009), suggest that the observed displacements are coherent with a NE-elongated sub-volcanic intrusions, localized on the upper part of the SdF (Casagli et al., 2009; Giordano and Porreca, 2009). The resulting bulging of the topographic surface is elongated parallel to the dyke strike, as well as faulting and fracturing occur with the same parallel strike (Gudmundsson and Loetveit, 2005).

Intrusions at Stromboli, once fed along the collapse axis from the upper rim of the SdF depression (Linde et al., 2014), mainly propagate within the collapse as the result of the deflection of the stress trajectories at the sides of the depression (Acocella and Tibaldi, 2005; Acocella and Neri, 2009; Neri et al., 2008; Tibaldi et al., 2008; Intrieri et al., 2013). Increase in magma overpressure, related to the volumetric expansion due to large gas flux from depth, promotes the lateral intrusion of sheets (Di Traglia et al., 2013; Nolesini et al., 2013). In the 2007 eruption, Vent 1 (650 m) was dyke-fed (NE–SW striking) and propagated further downslope to 400 m a.s.l. (Vent 2) and the variation in the direction of the dike-fed Vents 1 and 2 is supposed to be the result of the topography-induced deflection along the scar of the December 2002 landslide (Neri et al., 2008; Intrieri et al., 2013).

The NE-striking dyke also produces a lateral magma force exerted on the dyke walls in a SE–NW direction, as previously suggested by a number of authors (Apuani et al., 2005a,b, 2007 and references therein). This lateral force can enhance the gravity instability of the SdF infill. These intrusions can stop at depth, promoting the movement of part of the SdF seawards without the occurrence of ephemeral vents or landslides (Casagli et al., 2009; Nolesini et al., 2013).

6.2. Structural framework of the summit area

The GBInSAR data presented here allow the constraining of the structural setting of the summit crater area of Stromboli volcano. From the analysis of interferograms and cumulative displacement maps, a sharp boundary between the two main sectors of the outer flank of the crater terrace (sector 2 and 3) is evident. During the 2007 and 2012–13 crises, a strong increase in the displacement rate on sector 2 has been recorded two months and one month before the onset of the 2007 and the 2012–2013 crises, respectively. The increase in the displacement rate involved the entire sector 2, but in both cases the maximum displacement was located at the boundary between sector 2 and 3. This boundary could represent planes of weakness related to the collapse of the summit crater terrace.

During the 2007 crisis, the GBInSAR was able to record fluctuations in the displacement rate towards and backwards with respect to the sensor, interpreted as inflation-deflation of the uppermost volcanic system (Fig. 9). The inflations occurred before the opening of the effusive vents (27 February 2007; 9 March 2007), while deflation occurred in between the two events and after the second vent opening (Casagli et al., 2009). These two periods of deflations correspond to the incremental collapse of the summit crater area of Stromboli (Barberi et al., 2009). The 2007 crater collapse was associated with sudden increase in the number of earthquakes occurred on 7–8 March 2007 (about 60 events/h defined "hybrids" because of a frequency content of 4–5 Hz; Martini et al., 2007). Calvari et al. (2010) report the first observation of a summit crater collapse on 4 March, possibly occurred even earlier but hidden by clouds. A progressive fracturing was observed since 8 March 2007 until 13 March 2007 (Barberi et al., 2009), forming a collapse structure of a volume of about 1.5×10^6 m^3 (Marsella et al., 2009), with a thickness of the collapsed block in the range 80–150 m (Fig. 9; Neri and Lanzafame, 2009), giving an aspect ratio of 1.8 and a T/D ~0.5 (thickness/width ratio; Ruch et al., 2012). During the 2007 crisis, the downthrown motion of the northern portion of the SdF allowed the observation of the inner structure of the northern part of the summit area (Casagli et al., 2009). This is affected by a series of slip planes dipping towards the NW (i.e. towards the sea) at angles of 60°–80° and field observations indicate the presence of normal offsets (Casagli et al., 2009). As reported before, the GBInSAR recorded two cycles of displacements towards and backwards with respect to the sensor. In detail, the GBInSAR recorded an increase in the displacement rate away from the sensor (deflation) since the onset of the crisis (27 February 2007) until the 7 March 2007, when a large displacement rate toward the sensor have been registered in both the summit crater area and in the SdF (Casagli et al., 2009). The displacement vector inverted direction again after the re-opening of the effusive Vent 2 (400 m a.s.l.). The 2007 collapse of the summit crater area at Stromboli is in agreement with the experimental data of Ruch et al. (2012). For incremental collapse structure with T/D ratio < 2 and pre-existing collapse structure Ruch et al. (2012) suggested that the subsidence of the collapsing block is expected to be coupled with the rate of magma withdrawal, as observed at Stromboli (aspect ratio 0.13; Neri et al., 2008; Marsella et al., 2009). Moreover, even if the GBInSAR data revealed that the 2007 summit area started to subside soon after the onset of the effusive eruption (27 February) and the fracturing the crater terrace were observed on the 4 March (and possibly occurred earlier; Calvari et al., 2010), the larger part of the collapse occurred in few days, as suggested by the occurrence of the "hybrids" seismic signals (Martini et al., 2007). This is in agreement with the experimental data of Roche et al. (2001) for pit-craters with aspect ratio between 1 and 2. In these experiments, the initial sub surface collapse is followed by sudden roof collapse (Roche et al., 2001).

The presence of several slip zones that regulated the collapse of the summit crater area in the recent years has been yet recognized by Finizola et al. (2003) by means of geophysical and geochemical surveys (temperature, self-potential, CO_2 soil flux). The Pizzo slip zones are invoked to explain the geometry of the summit collapses (large pit crater formations) at Stromboli, while our GBInSAR data evidenced that the same structural features are also involved during the inflation-deflation fluctuations of the volcano.

The integration of GBInSAR, numerical modelling and structural field data, has been used to explain the ground deformation observed during the 2007 crisis. The pressurization of the shallow conduit system has been invoked to explain the observed deformations (Casagli et al., 2009). Increase in displacement rate in sector 2 (Fig. 4c) has been related to the increase in the magmastatic pressure within the conduit, as a consequence of the rise of the magma level (Fig. 9b), while the increase in the displacement rate in sector 3 (Fig. 4c) has been considered as the evidence of the pressurization and lateral expansion of the shallow conduit system of Stromboli volcano (Di Traglia et al., 2013, 2014a,b). In sector 3, increases in the displacement rate have been observed many times before the onset of the 2009–2013 crises (Di Traglia et al., 2013). Before the onset of the 2011 and 2012–13 crises, displacements were located in the lower part of sector 3 (600–650 m a.s.l.). During the 2012–13 crisis (Table 1), the localization of the displacements in sector 3 changed with time. Six days before (18 December 2012) the onset the maximum displacement rate was located near the top of the sector (700–750 m a.s.l.), while it lowered in elevation (650–700 m a.s.l.) during February-March 2013. Sector 3 corresponds to the opening area of the ephemeral vent of the 2002–03 and 2007 flank eruptions (Neri et al., 2008) and vent opening in sector 3 occurs when

the magma overpressure exceeds the rock stiffness (Casagli et al., 2009; Nolesini et al., 2013). The chronology of the onset of the 2012–13 crisis, in terms of inflation/NE-ward expansion of the summit area/deflation, resembles the sequence of events that occurred at the beginning of the 2007 crisis (inflation; eccentric effusion at the base of the NE crater; collapse of the summit area), suggesting a self-similar behaviour of the shallow-plumbing system at Stromboli volcano. During sheet propagation in a volcanic edifice, the energy release rate (energy available to drive fracture propagation; Gudmundsson, 2012) could change, depending on the type of boundary conditions applied and the sheet geometry. When the boundaries of a volcanic zone (in the Stromboli case it refers to the summit crater area) cannot move during an unrest period and sheet development, the only source of potential energy for the sheet development is the strain energy stored in the volcano before sheet propagation starts, mainly due to the stretching related to the extensional forces (Gudmundsson, 2009, 2011, 2012). The strain energy stored in the volcano is transformed into surface energy and largely dissipated during fracture propagation (Gudmundsson, 2012). Since no energy is added to the system during the fracture propagation, the strain energy decreases and the sheet stops. If the boundaries of the volcanic edifice can move during the fracture development, there are two principal sources of potential energy for the fracture development: the stored strain energy in the volcanic edifice and the work done by the external, generalized loading or force. The constant-displacement boundary conditions result in stable fracture propagation, i.e. as the fracture propagates the energy (stored strain energy) available to drive the fracture gradually decreases. Thus, constant-displacement boundary conditions favour comparatively small eruptions (for dykes), while constant-load boundary conditions result in an unstable fracture propagation, therefore favouring comparatively large eruptions. Horizontally propagating intrusions can only emplace if edifice load prevents eruption through the central area and if magma is negatively buoyant at shallow depth (Pinel and Jaupart, 2004; Di Traglia et al., 2013). In a volcanic edifice, at small distances from the feeder conduit axis, confining stresses act to prevent vertical propagation and a bulge develops at some distance from the focal area, which accounts for ephemeral vents in the SdF (Pinel and Jaupart, 2004; Di Traglia et al., 2013).

At Stromboli, the GBInSAR recorded a displacement rate in sector 2 of the same order of magnitude for both the 2007 and the 2012–13 crises. The peak in displacement rate during the 2007 eruption has been reached only during the ephemeral vent opening, i.e. when the magma overpressure was high enough to laterally propagate the conduit system forming a NE-SW striking dyke. During the (magmastatic) pressure built up of both eruptions, due to the rise of the magma level in the conduit, the existence of an upper limit of the displacement rate (<1 mm/h for the 2007 flank eruption) allowed us to speculate that the initial phases of Stromboli eruptions are characterized by a constant load (the flanks of the summit crater area can expand during pressure build-up), while, reaching the displacement rate of 0.7–0.8 mm/h, the boundary conditions change and the sheet propagation occurs at fixed boundary (constant displacement) condition. This implies that, if there is no magma overpressure (due to pressurization of the HP-filled conduit related here to the degassing of the LP magma; Di Traglia et al., 2013) or weakening of the country rocks, the fractures no longer propagate, preventing the development of a flank effusion. Magma pressure (p_{tot}) acting on the dyke consists of the magma-static (p_m) and an overpressure (p_o) components (Voight and Elsworth, 1997; Apuani and Corazzato, 2009). The maximum magmastatic pressure component, responsible of the upper limit of the displacement rate in sector 2, can be easily evaluated considering the variation of the magma level within the Stromboli conduit. The magmastatic pressure can be calculated as:

$$p_m = \boldsymbol{\gamma}_m \cdot z$$

Where $\boldsymbol{\Upsilon_m}$ and z are the average magma unit weight (25.5 kN/m^3; Barberi et al., 1993) and the height of the dyke, respectively. Calculating the pressure variation at different heights, considering the change in the elevation of the maximum displacement in sector 3 (max. 100 m), the change in the magma-static pressure related to the rise of the magma level of about 2 MPa can be evaluated.

The magma overpressure responsible for the lateral propagation can be evaluated considering that magma flow in a sheet intrusion can be driven by the excess magma pressure at the source, the magma buoyancy and the gradients of the 'tectonic' stress normal to the sheet plane (Rubin, 1995). Di Traglia et al. (2013) and Nolesini et al. (2013) proposed a range of magma overpressures characterizing both the 2009–2013 crises and the 2007 flank eruption, considering the 'tectonic' stress normal to the sheet plane to be constant (no strong earthquake in the considering period). Local stress configuration, e.g. due to changes in morphology, could control the direction and geometry of emplacement of the intrusion, as extensively demonstrated at Stromboli around the SdF after sector collapses (Tibaldi, 2001, 2003; Tibaldi et al., 2009). However, during the investigated period, the morphological changes of sector 3 were not likely to redefine the orientation of the local stress. Magma buoyancy can be neglected because it generally affects the vertical propagation of intrusion (magmastatic pressure), rather than a lateral propagation (Rubin, 1995). Considering these assumptions and limitations and using the deformation rate as a proxy for the order of magnitude of the sheet propagation rate (U), the magma overpressure (p_o) needed to generate the registered deformation rates can be evaluated by:

$$U = lp_o^3/3\eta M^2$$

where M is the host rock elastic stiffness, $\boldsymbol{\eta}$ is the magma viscosity and $\boldsymbol{l}$ is the intrusion length (Rubin, 1995). Regarding the host rock elastic stiffness, we chose the range of 10–20 GPa proposed by Apuani et al. (2005a,b) and Rotonda et al. (2010) and not considering possible local variations (Thomas et al., 2004; Gudmundsson, 2011). This assumption is based on the observations made on the lithic ejected during the paroxysmal explosions, considered as samples of the host rocks of the shallow conduit system (Pistolesi et al., 2008), considered as samples of the country rock bounding the shallow conduit system. Ballistic blocks are quite different: the SW crater mainly produces hydrothermally altered fragments, material altered from fumarolic activity and vesicular altered lavas (Del Moro et al., 2013), likely representing the brittle failure of the conduit wall rocks due to the ascent of an overpressurized gas-slug (Rosi et al., 2006). In the other hand, the NE crater produces fresh, holocrystalline subvolcanic blocks, representing the slowly cooled equivalents of the HP magmas feeding the normal Strombolian explosions (Pistolesi et al., 2008; Renzulli et al., 2009).

The HP magma viscosity is in the order of 104–105 Pa · s (Vona et al., 2011) and the intrusion length is in the interval of 100–300 m, considered as the distance between the in-depth projection of the NE crater conduit and the tip of the intrusion, allowing for both the error in the exact location of the conduit and in the intrusion depth (Chouet et al., 2003). Overpressures were obtained on the order of 10^{-2} MPa for a low displacement rate in sector 3 (<0.1 mm/h), 10^{-1} MPa for displacement rates typical for the crises dominated by overflows and major explosions (0.1–10 mm/h) and 10^0–10^1 MPa for the high displacement rate (>10 mm/h) as during the 2007 and 2012–13 crisis. In this scenario, the observed long-term (monthly) fluctuations of ground displacement (the high-displacement rate that characterized each crisis) can be related to cyclic pressurisation phases of the magma column within the feeding system by gas-rich magma (Coppola et al., 2012). At the same time, short-term fluctuation in the displacement rate, as revealed by Di Traglia et al. (2014a,b), could reflect short-term pressurization events on a time scale of minutes or hours, that produces fluctuations in degassing and explosive activity (Coppola et al., 2012).

An alternative explanation of the difference between the 2007 flank eruption and the post–2007 crises have been proposed by Coppola et al. (2012, 2014) and Calvari et al. (2014). These authors observed a different behaviour in the eruptive activity between during the 2005–2006 (pre-2007 crises) and 2008–2012 (post-2007 crises) periods. They suggested that this is an indication that the uprising of magma, and its storage at shallow levels, was markedly perturbed by the February 2007 eruption (Coppola et al., 2014). Calvari et al. (2014) support this hypothesis using SO_2 and CO_2 recorded from the plume, coupled with the temperature recorded at low-elevation fumaroles. They observed that the increase in the number of lava overflows and major explosions is not related to anomalously high supplies of gas-rich magma rising along the conduit. Calvari et al. (2014) thus suggest that the observed geochemical trends are due to the increased capacity of the uppermost conduit to accommodate a larger amount of magma in an articulated fingering system developed beneath the craters, formed after the 2007 collapse of the crater area.

These two scenarios are not opposed. In fact, the 2007 collapse of the crater area likely affected the very shallow plumbing system at Stromboli, increasing the magma volume that can be accumulated beneath the crater terrace and then increasing the limit of the displacement rate for the constant load/constant displacement transition. This processes will have in turn decreased the occurrence of large lava flows, compared with overflows (Coppola et al., 2012, 2014; Calvari et al., 2014), decreasing the ability to decompress the deeper storage system, triggering the ascent of the gas-rich magma responsible of the paroxysmal explosions (Aiuppa et al., 2009, 2010; Calvari et al., 2011b). As stated by Calvari et al. (2014), this process will probably eventually end with the restoration of the previous central conduit path, mainly by the thermal erosion that normally acts beneath the Stromboli crater terrace (Del Moro et al., 2013).

Meanwhile, pre- and post-2007 plume CO_2/SO_2 ratio was similar for both inter-crises and crises periods (Aiuppa et al., 2009, 2010, 2011; La Spina et al., 2013) testifying that the same processes of shallow magma degassing occurred, supporting the short-term fluctuation in the displacement rate during each eruptive crisis recorded by the GB-InSAR system (Di Traglia et al., 2014a,b).

6.3. Changing in eruption intensity at Stromboli volcano

On a long-time scale, the GBInSAR recorded a fluctuating behaviour of the summit crater area (mainly sector 2), with periods of increases in the displacement rate that anticipated and accompanied the volcanic crisis and a reduction in the displacement rate following the crisis. During a single period of higher volcanic activity, fluctuations have been also recorded in a shorter time scale (days to weeks). Similar results have been obtained from the analysis of other geophysical and geochemical parameters. In particular, Coppola et al. (2012, 2014), comparing the number of explosions (Very Long Periods seismic events) per day with the radiative power emitted by Stromboli craters and detected by MODIS (Moderate Resolution Imaging Spectroradiometer) satellite observations, suggested that over the years 2000–2011 several fluctuations of rise and fall of the magma column (revealed by intermediate to high radiative power) have occurred. Only two rises of the magma column culminated in effusive crisis (2002–03 and 2007), while the other periods did not evolve with lava effusion but only into episodes of sustained spattering or fountaining and summit overflows (lava lake behaviour; Coppola et al., 2012).

The geochemical monitoring network recognized similar results. Major explosions activity clusters in periods preceded by brief phases of increasing CO_2/SO_2 weight ratio (up to > 40) and CO_2 flux (>1300 $t \cdot d^{-1}$) with respect to the time averaged values of 3.7 and 500 $t \cdot d^{-1}$ typical for standard Stromboli's activity. On the other hand, paroxysmal explosions and flank effusive eruptions occurred at higher CO_2/SO_2 ratio (up to 21; Aiuppa et al., 2009). It is worth noticing that high CO_2/SO_2 ratios are strongly related to the deeper source, while lower CO_2/SO_2 ratios reflect a stronger contribution from magma degassing within the shallow conduit system (La Spina et al., 2013).

Fluctuations in the displacement rate are related to variations in flow rate through the shallow conduit system and thus to the rise speed of the magma beneath the vent (Parfitt, 2004). Variation in magma flow rate can be explained by magma convection within the plumbing system of Stromboli (Burton et al., 2007a,b; Witham, 2011) and the increasing gas content of the magma induces a faster rate of magma convection (Aiuppa et al., 2010). High magma column occurs when the rate of magma supplied at depth and degassing within the feeding system is balanced by an equal amount of lava discharged at the vents or degassed magma is cycled back within the conduit (typically 0.3 $m^3 \cdot s^{-1}$ at Stromboli; Allard et al., 1994; Coppola et al., 2012). A higher supply rate is necessary to shift the eruptive intensity to a higher level, promoting the occurrence of eccentric effusive and/or paroxysmal activity (Allard et al., 1994; Coppola et al., 2012). According to Lautze and Houghton (2005, 2007), magmas with different vesicularity may reside in the upper part of Stromboli's conduit system and the relative abundance are due to on-going vesiculation and mixing/mingling of different magmas. Variations in magma density have been mainly related to the density-driven overturning due to the gas transfer from the deeper level to the HP magma residing in the shallow (<1 km) plumbing system of Stromboli volcano (Lautze and Houghton, 2005, 2007; Burton et al., 2007a,b; Aiuppa et al., 2009, 2010; Witham, 2011). In fact, CO_2-rich gas bubbles are persistently supplied to the shallow plumbing system by degassing (and gas-melt separation) in the LP magma storage zone. If the rate of supply of CO_2-rich gas bubbles to the shallow plumbing system is low, the close-to-surface gas–melt separation from the shallow-convecting magma likely sustains the surface gas emissions (Aiuppa et al., 2009). Moreover, density changes can be also explained by the rise of the high-vesicular LP magma from 7–10 km deep (D'Oriano et al., 2011; Carbone et al., 2012). In this context, the rise and fall of the displacement rate in sector 2 can be related to the magma overturning within the conduit, with the increases in displacement rate during the upwelling of less dense magma. The displacement rate in sector 2 decreases as the degassed magma column is pushed out from the conduit due to the rising of volatile-rich magma. Instead, the decrease in the displacement rate without coeval lava outpouring (lava flows or overflows) could be related to the sink of the degassed magma due to density contrast between the volatile poor and the volatile-rich magmas.

6.4. The GBInSAR monitoring system: a tool for mitigating the risk connected with intense eruptive activity and flank dynamics at Stromboli volcano

As reported before, flank dynamics at Stromboli volcano is continuous, characterized by the near constant seaward movement of the Sciara del Fuoco flank. Tibaldi et al. (2009) suggest that the contrast of the rheological properties between the consolidated pre-collapse rocks and the successive looser infill of the collapse depression, together with the existence of other discontinuities (buried collapse scarps and related fractures), are predisposing factors for gravitational instability in the Sciara del Fuoco. Deformation occurs through creep and space is created along the lateral margins of the unstable sector through transtensional slip of the unstable sector. During this stage, rising magma can escape from the central feeding zone creating sheets along the lateral margins of the unstable sector (Tibaldi et al., 2009). This implies that, after a period of creep movements, sheet emplacement can occur during a stage of magma upwelling under increased magma pressure (Tibaldi et al., 2009).

Thus, while flank dynamics of Stromboli volcano is a steady state process, flank unrest is defined as any acceleration of the Sciara del Fuoco and may be related to hazardous conditions as flank eruptions, surface fracturing and tsunamigenic landslides. Flank unrests at Stromboli produce distinct structural, geophysical and volcanological evidences (Barberi et al., 2009). Movements of the Sciara del Fuoco

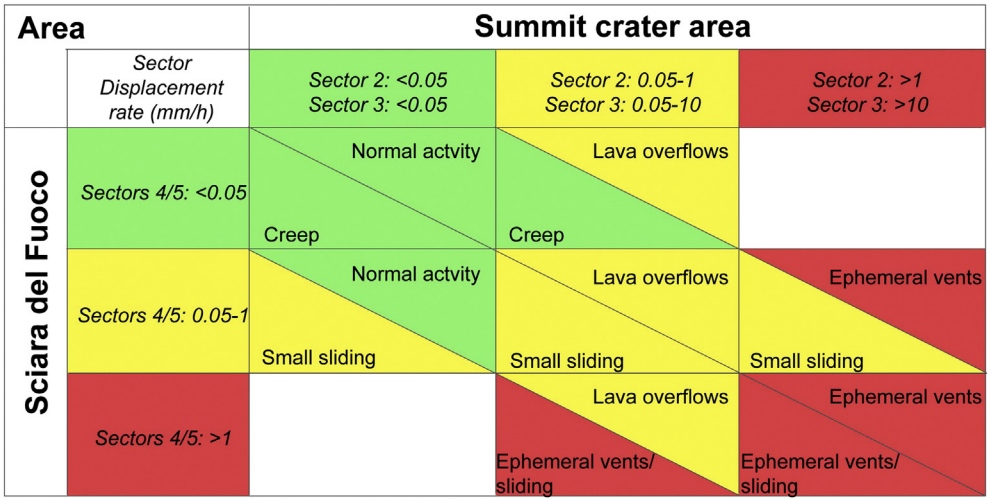

Fig. 10. Representative diagram for Stromboli unrest as operation tool for the mitigation of the Sciara del Fuoco dynamics and the increase in explosive activity. Different threshold are based on the back-analysis of the 2003–2013 GBInSAR time series.

produced variations of the patterns of the surface displacements (Antonello et al., 2004; La Rocca et al., 2004; Bonforte et al., 2008; Casagli et al., 2009; Marchetti et al., 2009), while are generally anticipated by changes in the eruptive activity, increases in the displacement rate in the summit area and variations in the geochemical parameters. As an example, the increase in displacement rate in sector 2 and in the CO_2/SO_2 ratios anticipated the onset of the 2007 crisis by two weeks. Given these strong relationships between changes in the eruptive behaviour (and the associated geophysical and geochemical parameters) with the flank eruptions in the Sciara del Fuoco, we define a scenario for the flank unrest at Stromboli (Fig. 10). Using the displacement rate in sector 2 and 3 as a proxy for the variation in the magmastatic pressure in conduit and for magma overpressure, respectively, thresholds for the crises characterized by the occurrence of overflows (eventually associated with major explosions) and flank effusions (eventually associated with paroxysmal explosions) could be identified. Early increases in displacement rate in sector 3, testifying the variations in the pressure condition within the conduit due to CO_2 released from depth (Di Traglia et al., 2013), generally anticipate the onset of an anomalous phase. Increases in the displacement rate in sector 2, testifying the increase in the magmastatic pressure due to the rise of the magma level within the Stromboli conduit with constant load boundary conditions, anticipated the more intense phases of volcanic activity. During a single crisis, newly increases in the displacement rate in sector 3, during phases of lateral conduit propagation at fixed boundary (constant displacement) condition, may anticipate the onset of effusive activity. Small conduit overpressure will produce overflows (sometimes associated with crater-rim collapses), while large magma overpressure will laterally expand the conduit forming a NE-SW striking dyke, feeding eruptive vents at the base of the summit crater area. Otherwise, the onset of flank unrest could be evaluated by monitoring the displacement rate in the SdF. Accelerations in this sector are related to sheet intrusions, while the possibility of vent opening, associated with small sliding, or catastrophic flank failure are related to high overpressurized sheets, able to produce high displacement rate in the SdF. Unfortunately, the GBInSAR system is able to monitor only the N portion of the Sciara del Fuoco. Intrusions in the southern sector of the SdF would not be anticipated without the placement of another GBInSAR system on the S slope.

7. Conclusions

The GBInSAR system has been used to monitor the slope instability in the northern sector of the SdF and also to detect the inflation and deflation of the N sector of the crater area, allowing us to define the unstable area within the SdF and also to outline the structural framework of the summit area.

This work is the attempt to formalize the knowledge of the GBInSAR monitoring group gained from the last decade of monitoring activity and it is based on the conceptual model for flank dynamics and unrests at Mt. Etna proposed by Acocella and Puglisi (2013). This scenario is centred on the assumption that any potential event occurring in the future shows precursory displacement rates similar to those witnessed for the same event in the last 10 years. The main limitations are related to relatively short monitoring time period (10 years) on which our scenarios are based and hence the temporal extent for the applicability of this scenario (years to few decades). As an example, data on the preparatory phase of large (Sciara del Fuoco-forming collapse; Tibaldi, 2001) to moderate (30 December 2002-like event; Tommasi et al., 2005) slope failure, as well as the preparatory phase of a large paroxysm period (1930-like event; Bertagnini et al., 2011), are still lacking. Moreover, the flank unrest scenario proposed here relies only on the GBInSAR displacement data, based on the observations available for the last 10 years at Stromboli, while a more complete scenario needs an integrated approach merging volcanological, geochemical and the other geophysical parameters (seismic, GPS, tilt, accelerometers, etc). Furthermore, the biggest limitation to this work is the spatial coverage of the GBInSAR data. A larger area of the SdF and of the summit crater area (using a GBInSAR system in the southern edge of the Sciara del Fuoco) is necessary to create a complete displacement model for Stromboli volcano.

Acknowledgments

This work has been sponsored in part by the National Civil Protection Department (DPC) within the framework of the SAR.net, SAR.net2 and InGrID projects and through the Istituto Nazionale di Geofisica e Vulcanologia and DPC Stromboli emergency Project V2. The DPC is acknowledged for supporting the project and permitting this publication. The authors are grateful to Carlo Rivolta and Ivan Binda Rossetti (Ellegi s.r.l. – Lisalab) for the technical support during the eruptive crises. The authors are grateful to A. Tibaldi (UniMiB) for his review and to G.R. Foulger for the editorial management. Sonia Calvari (INGV-OE) is greatly acknowledged for her revisions, discussions and comments. FeDiT is supported by a post-doc fellowship founded by the Regione Toscana (UNIPI-FSE) under the project "*Space-born and ground-based SAR techniques for the evaluation of natural hazard*" (RadSafe – UNIPI-4) in the framework of the research agreement between DST-UNIPI, DST-UNIFI and Ellegi s.r.l. Lisalab.

References

Acocella, V., Tibaldi, A., 2005. Dike propagation driven by volcano collapse: a general model tested at Stromboli, Italy. Geophys. Res. Lett. 32 (8).

Acocella, V., Neri, M., 2009. Dike propagation in volcanic edifices: overview and possible developments. Tectonophysics 471 (1), 67–77.

Acocella, V., Puglisi, G., 2013. How to cope with volcano flank dynamics? A conceptual model behind possible scenarios for Mt. Etna. J. Volcanol. Geotherm. Res. 251, 137–148.

Aiuppa, A., Federico, C., Giudice, G., Giuffrida, G., Guida, R., Gurrieri, S., Liuzzo, M., Moretti, R., Papale, P., 2009. The 2007 eruption of Stromboli volcano: insights from real-time measurements of the volcanic gas plume CO_2/SO_2 ratio. J. Volcanol. Geotherm. Res. 182, 221–230.

Aiuppa, A., Burton, M., Caltabiano, T., Giudice, G., Guerrieri, S., Liuzzo, M., Mure, F., Salerno, G., 2010. Unusually large magmatic CO_2 gas emissions prior to a basaltic paroxysm. Geophys. Res. Lett. 37, L17303.

Aiuppa, A., Burton, M., Allard, P., Caltabiano, T., Giudice, G., Gurrieri, S., Liuzzo, M., Salerno, G., 2011. First observational evidence for the CO_2-driven origin of Stromboli's major explosions. Solid Earth 2, 135–142.

Allard, P.A., 2010. CO_2-rich gas trigger of explosive paroxysms at Stromboli volcano, Italy. J. Volcanol. Geotherm. Res. 189, 363–374.

Allard, P., Carbonelle, J., Metrich, N., Loyer, H., Zettwoog, P., 1994. Sulfur output and magma degassing budget of Stromboli volcano. Nature 368 (6469), 326–330.

Andronico, D., Corsaro, R.A., Cristaldi, A., Polacci, M., 2008. Characterizing high energy explosive eruptions at Stromboli volcano using multidisciplinary data: An example from the 9 January 2005 explosion. J. Volcanol. Geotherm. Res. 176, 541–550.

Andronico, D., Taddeucci, J., Cristaldi, A., Miraglia, L., Scarlato, P., Gaeta, M., 2013. The 15 March 2007 paroxysm of Stromboli: video-image analysis, and textural and compositional features of the erupted deposit. Bull. Volcanol. 75, 733.

Antonello, G., Casagli, N., Farina, P., Leva, D., Nico, G., Sieber, A.J., Tarchi, D., 2004. Ground-based SAR interferometry for monitoring mass movements. Landslides 1, 21–28.

Apuani, T., Corazzato, C., 2009. Numerical model of the Stromboli volcano (Italy) including the effect of magma pressure in the dyke system. Rock Mech. Rock. Eng. 42, 53–72.

Apuani, T., Corazzato, C., Cancelli, A., Tibaldi, A., 2005a. Physical and mechanical properties of rock masses at Stromboli: a dataset for flank instability evaluation. Bull. Eng. Geol. Environ. 64, 419–432.

Apuani, T., Corazzato, C., Cancelli, A., Tibaldi, A., 2005b. Stability of a collapsing volcano (Stromboli–Italy): limit equilibrium analysis and numerical modelling. In: Gudmundsson, A., Acocella, V. (Eds.), The tectonics and physics of volcanoes. Special issue. J. Volcanol. Geotherm. Res. 144, pp. 191–210.

Apuani, T., Merri, A., Masetti, M., 2007. In International Workshop on Volcanic Rocks, 11th ISRM Congress. Effects of volcanic seismic events on the Stromboli stability by finite difference numerical modeling. Taylor & Francis/Balkema.

Arrighi, S., Rosi, M., Tanguy, J.-C., Courtillot, V., 2004. Recent eruptive history of Stromboli (Aeolian Islands, Italy) determined from high accuracy archeomagnetic dating. Geophys. Res. Lett. 31, L19603.

Baldi, P., Coltelli, M., Fabris, M., Marsella, M., Tommasi, P., 2008. High precision photogrammetry for monitoring the evolution of the NW flank of Stromboli volcano during and after the 2002–2003 eruption. Bull. Volcanol. 70 (6), 703–715.

Barberi, F., Rosi, M., Sodi, A., 1993. Volcanic hazard assessment at Stromboli based on review of historical data. Acta Vulcanol. 3, 173–187.

Barberi, F., Civetta, L., Rosi, M., Scandone, R., 2009. Chronology of the 2007 eruption of Stromboli and the activity of the Scientific Synthesis Group. J. Volcanol. Geotherm. Res. 182, 123–130.

Bertagnini, A., Landi, P., 1996. The Secche di Lazzaro pyroclastics of Stromboli volcano: a phreatomagmatic eruption related to the Sciara del Fuoco sector collapse. Bull. Volcanol. 58, 239–245.

Bertagnini, A., Di Roberto, A., Pompilio, M., 2011. Paroxysmal activity at Stromboli: lessons from the past. Bull. Volcanol. 73, 1229–1243.

Blackburn, E.A., Wilson, L., Sparks, R.S.J., 1976. Mechanisms and dynamics of Strombolian activity. J. Geol. Soc. Lond. 132, 429–440.

Boldini, D., Wang, F., Sassa, K., Tommasi, P., 2009. Application of large-scale ring shear tests to the analysis of tsunamigenic landslides at the Stromboli volcano, Italy. Landslides 6, 231–240.

Bonaccorso, A., 1998. Evidence of a dyke-sheet intrusion at Stromboli volcano inferred through continuous tilt. Geophys. Res. Lett. 25 (22), 4225–4228.

Bonaccorso, A., Davis, P.M., 1999. Models of ground deformation from vertical volcanic conduits with application to eruptions of Mount St. Helens and Mount Etna. J. Geophys. Res. Solid Earth (1978–2012) 104 (B5), 10531–10542.

Bonaccorso, A., Calvari, S., Garfì, G., Lodato, L., Patanè, D., 2003. Dynamics of the December 2002 flank failure and tsunami at Stromboli volcano inferred by volcanological and geophysical observations. Geophys. Res. Lett. 30 (18).

Bonaccorso, A., Gambino, S., Guglielmino, F., Mattia, M., Puglisi, G., Boschi, E., 2008. Stromboli 2007 eruption: Deflation modeling to infer shallow-intermediate plumbing system. Geophys. Res. Lett. 35, L06311.

Bonaccorso, A., Bonforte, A., Gambino, S., Mattia, M., Guglielmino, F., Puglisi, G., Boschi, E., 2009. Insight on recent Stromboli eruption inferred from terrestrial and satellite ground deformation measurements. J. Volcanol. Geotherm. Res. 182, 172–181.

Bonaccorso, A., Calvari, S., Linde, A., Sacks, S., Boschi, E., 2012. Dynamics of the shallow plumbing system investigated from borehole strainmeters and cameras during the 15 March, 2007 Vulcanian paroxysm at Stromboli volcano. Earth Planet. Sci. Lett. 357–358, 249–256.

Bonforte, A., Aloisi, M., Antonello, G., Casagli, N., Fortuny-Guash, J., Guerri, L., Nunnari, G., Puglisi, G., Spata, A., Tarchi, D., 2008. Movements of the Sciara del Fuoco. In: Calvari, S., Inguaggiato, S., Puglisi, G., Ripepe, M., Rosi, M. (Eds.), The Stromboli volcano: an integrated study of the 2002–2003 eruption. American Geophysical Union Monograph Series 182, pp. 183–199.

Burton, M.R., Allard, P., Murè, F., La Spina, A., 2007a. Magmatic gas composition reveals the source depth of slug-driven Strombolian explosive activity. Science 317, 227–230.

Burton, M.R., Mader, H.M., Polacci, M., 2007b. The role of gas percolation in quiescent degassing of persistently active basaltic volcanoes. Earth Planet. Sci. Lett. 264, 46–60.

Burton, M.R., Caltabiano, T., Murè, F., Salerno, G., Randazzo, D., 2009. SO< sub> 2 flux from Stromboli during the 2007 eruption: Results from the FLAME network and traverse measurements. J. Volcanol. Geotherm. Res. 182 (3), 214–220.

Calvari, S., Spampinato, L., Lodato, L., Harris, A.J.L., Patrick, M.R., Dehn, J., Burton, M.R., Andronico, D., 2005. Chronology and complex volcanic processes during the 2002–2003 flank eruption at Stromboli volcano (Italy) reconstructed from direct observations and surveys with a handheld thermal camera. J. Geophys. Res. Solid Earth 110 (B2).

Calvari, S., Lodato, L., Steffke, A., Cristaldi, A., Harris, A.J.L., Spampinato, L., Boschi, E., 2010. The 2007 Stromboli eruption: Event chronology and effusion rates using thermal infrared data. J. Geophys. Res. B04201 http://dx.doi.org/10.1029/2009JB006478.

Calvari, S., Büttner, R., Cristaldi, A., Dellino, P., Giudicepietro, F., Orazi, M., Peluso, R., Spampinato, L., Zimanowski, B., Boschi, E., 2011a. The 7 September 2008 Vulcanian explosion at Stromboli volcano: Multiparametric characterization of the event and quantification of the ejecta. J. Geophys. Res. 117 (B5), B05201.

Calvari, S., Spampinato, L., Bonaccorso, A., Oppenheimer, C., Rivalta, E., Boschi, E., 2011b. Lava effusion – A slow fuse for paroxysms at Stromboli volcano? Earth Planet. Sci. Lett. 301, 317–323.

Calvari, S., Branca, S., Corsaro, R.A., De Beni, E., Miraglia, L., Norini, G., Wijbrans, J., Boschi, E., 2011c. Reconstruction of the eruptive activity on the NE sector of Stromboli volcano: timing of flank eruptions since 15 ka. Bull. Volcanol. 73, 101–112.

Calvari, S., Büttner, R., Cristaldi, A., Dellino, P., Giudicepietro, F., Orazi, M., Peluso, R., Spampinato, L., Zimanowski, B., Boschi, E., 2012. The 7 September 2008 Vulcanian explosion at Stromboli volcano: Multiparametric characterization of the event and quantification of the ejecta. J. Geophys. Res. 117, B05201. http://dx.doi.org/10.1029/2011JB009048 B05201.

Calvari, S., Bonaccorso, A., Madonia, P., Neri, M., Liuzzo, M., Salerno, G.G., Behncke, B., Caltabiano, T., Cristaldi, A., Giuffrida, G., La Spina, A., Marotta, E., Ricci, T., Spampinato, L., 2014. Major eruptive style changes induced by structural modifications of a shallow conduit system: the 2007–2012 Stromboli case. Bull. Volcanol. 76, 841.

Carbone, D., Zuccarello, L., Montalto, P., Rymer, H., 2012. New geophysical insight into the dynamics of Stromboli volcano (Italy). Gondwana Res. 22, 290–299.

Casagli, N., Tibaldi, A., Merri, A., Del Ventisette, C., Apuani, T., Guerri, L., Fortuny-Guasch, J., Tarchi, D., 2009. Deformation of Stromboli Volcano (Italy) during the 2007 crisis by radar interferometry, numerical modeling and field structural data. J. Volcanol. Geotherm. Res. 182, 182–200.

Casagli, N., Catani, F., Del Ventisette, C., Luzi, G., 2010. Monitoring, prediction and early warning using ground-based radar interferometry. Landslides 7, 291–301.

Chaussard, E., Amelung, F., Aoki, Y., 2013. Characterization of open and closed volcanic systems in Indonesia and Mexico using InSAR time series. J. Geophys. Res. Solid Earth 118 (8), 3957–3969.

Chiocci, F.L., Romagnoli, C., Tommasi, P., Bosman, A., 2008. The Stromboli 2002 tsunamigenic submarine slide: characteristics and possible failure mechanisms. J. Geophys. Res. 113, B10102.

Chouet, B., Dawson, P., Ohminato, T., Martini, M., Saccorotti, G., Giudicepietro, F., Scarpa, R., 2003. Source mechanisms of explosions at Stromboli Volcano, Italy, determined from moment-tensor inversions of very-long-period data. J. Geophys. Res. Solid Earth (1978–2012) 108 (B1), ESE-7.

Coppola, D., Piscopo, D., Laiolo, M., Cigolini, C., Delle Donne, D., Ripepe, M., 2012. Radiative heat power at Stromboli volcano during 2000–2011: Twelve years of MODIS observations. J. Volcanol. Geotherm. Res. 215–216, 48–60.

Coppola, D., Laiolo, M., Delle Donne, D., Ripepe, M., Cigolini, C., 2014. Hot-spot detection and characterization of strombolian activity from MODIS infrared data. Int. J. Remote Sens. 35 (9), 3403–3426.

Del Bello, E., Llewellin, E.W., Taddeucci, J., Scarlato, P., Lane, S.J., 2012. An analytical model for gas overpressure in slug-driven explosions: insights into Strombolian volcanic eruptions. J. Geophys. Res. 117, B02206.

Del Moro, S., Renzulli, A., Landi, P., La Felice, S., Rosi, M., 2013. Unusual lapilli tuff ejecta erupted at Stromboli during the 15 March 2007 explosion shed light on the nature and thermal state of rocks forming the crater system of the volcano. J. Volcanol. Geotherm. Res. 254, 37–52.

Di Roberto, A., Bertagnini, A., Pompilio, M., Gamberi, F., Marani, M.P., Rosi, M., 2008. Newly discovered submarine flank eruption at Stromboli volcano (Aeolian Islands, Italy). Geophys. Res. Lett. 35, 16.

Di Roberto, A., Rosi, M., Bertagnini, A., Marani, M.P., Gamberi, F., 2010. Distal turbidites and tsunamigenic landslides of Stromboli volcano (Aeolian Islands, Italy). Submarine mass movements and their consequences. Adv. Nat. Technol. Hazards Res. 28, 719–731.

Di Roberto, A., Bertagnini, A., Pompilio, M., Bisson, M., 2014. Pyroclastic density currents at Stromboli volcano (Aeolian Islands, Italy): a case study of the 1930 eruption. Bull. Volcanol. 76 (6), 1–14.

Di Traglia, F., Del Ventisette, C., Mugnai, F., Intrieri, E., Rosi, M., Moretti, S., Casagli, N., 2013. Ground Based InSAR reveals conduit pressurization pulses at Stromboli volcano. Terra Nova 25, 192–198.

Di Traglia, F., Intrieri, E., Nolesini, T., Bardi, F., Del Ventisette, C., Ferrigno, F., Frangioni, S., Frodella, W., Giglio, G., Lotti, A., Tacconi Stefanelli, C., Tanteri, L., Leva, D., Casagli, N., 2014a. The ground-based InSAR monitoring system at Stromboli volcano: linking changes in displacement rate and intensity of persistent volcanic activity. Bull. Volcanol. 76, 1–18.

Di Traglia, F., Cauchie, L., Casagli, N., Saccorotti, G., 2014b. Decrypting geophysical signals at Stromboli Volcano (Italy): integration of seismic and Ground-Based InSAR displacement data. Geophys. Res. Lett. http://dx.doi.org/10.1002/2014GL059824.

D'Oriano, C., Bertagnini, A., Pompilio, M., 2011. Ash erupted during normal activity at Stromboli (Aeolian Islands, Italy) raises questions on how the feeding system works. Bull. Volcanol. 73, 471–477.

Falsaperla, S., Maiolino, V., Spampinato, S., Jaquet, O., Neri, M., 2008. Sliding episodes during the 2002–2003 Stromboli lava effusion: insights from seismic, volcanic, and statistical data analysis. Geochem. Geophys. Geosyst. 9 (4).

Finizola, A., Sortino, F., Lénat, J.F., Valenza, M., 2002. Fluid circulation at Stromboli Volcano (Aeolian Islands, Italy) from self-potential and CO_2 surveys. J. Volcanol. Geotherm. Res. 116, 1–18.

Finizola, A., Sortino, F., Lénat, J.F., Aubert, M., Ripepe, M., Valenza, M., 2003. The summit hydrothermal system of Stromboli. New insights from self-potential, temperature, CO2 and fumarolic fluid measurements, with structural and monitoring implications. Bull. Volcanol. 65, 486–504.

Ghiglia, D.C., Romero, L.A., 1994. Robust two-dimensional weighted and unweighted phase unwrapping that uses fast transforms and iterative methods. JOSA A 11 (1), 107–117.

Gillot, P.Y., Keller, J., 1993. Radiochronological dating of Stromboli. Acta Vulcanol. 3, 69–77.

Giordano, G., Porreca, M., 2009. Field observations on the initial lava flow and the fracture system developed during the early days of the Stromboli 2007 eruption. J. Volcanol. Geotherm. Res. 182, 145–154.

Giudicepietro, F., D'Auria, L., Martini, M., Caputo, T., Peluso, R., De Cesare, W., Orazi, M., Scarpato, G., 2009. Changes in the VLP seismic source during the 2007 Stromboli eruption. J. Volcanol. Geotherm. Res. 182 (3), 162–171 (Italy).

Goto, A., Ripepe, M., Lacanna, G., 2014. Wideband acoustic records of explosive volcanic eruptions at Stromboli: New insights on the explosive process and the acoustic source. Geophys. Res. Lett. 41 (11), 3851–3857 (16 June).

Gudmundsson, A., 2009. Toughness and failure of volcanic edifices. Tectonophysics 471, 27–35.

Gudmundsson, A., 2011. Deflection of dykes into sills at discontinuities and magma-chamber formation. Tectonophysics 500, 50–64.

Gudmundsson, A., 2012. Strengths and strain energies of volcanic edifices. Nat. Hazards Earth Syst. Sci. 12, 2241–2258.

Gudmundsson, A., Loetveit, I.F., 2005. Dyke emplacement in a layered and faulted rift zone. J. Volcanol. Geotherm. Res. 144, 311–327.

Gurioli, L., Colo, L., Bollasina, A.J., Harris, A.J.L., Whittington, A., Ripepe, M., 2014. Dynamics of Strombolian explosions: inferences from field and laboratory studies of erupted bombs from Stromboli volcano. J. Geophys. Res. Solid Earth 119 (1), 319–345.

Hornig-Kjarsgaard, I., Keller, J., Koberski, U., Stadlbauer, E., Francalanci, L., Lenhart, R., 1993. Geology, stratigraphy and volcanological evolution of the island of Stromboli, Aeolian arc, Italy. Acta Vulcanol. 3, 21–68.

Houghton, B.F., Swanson, D.A., Rausch, J., Carey, R.J., Fagents, S.A., Orr, T.R., 2013. Pushing the Volcanic Explosivity Index to its limit and beyond: Constraints from exceptionally weak explosive eruptions at Kīlauea in 2008. Geology 41, 627–630.

Hougthon, B.F., Gonnermann, H.M., 2008. Basaltic explosive volcanism: constraints from deposits and models. Chem. Erde Geochem. 68, 117–140.

Hurlimann, M., Ledesma, A., Martı, J., 2001. Characterisation of a volcanic residual soil and its implications for large landslide phenomena: application to Tenerife, Canary Islands. Eng. Geol. 59, 115–132.

Inguaggiato, S., Vita, F., Rouwet, D., Bobrowski, N., Morici, S., Sollami, A., 2011. Geochemical evidence of the renewal of volcanic activity inferred from CO_2 soil and SO_2 plume fluxes: the 2007 Stromboli eruption (Italy). Bull. Volcanol. 73, 443–456.

Intrieri, E., Di Traglia, F., Del Ventisette, C., Gigli, G., Mugnai, F., Luzi, G., Casagli, N., 2013. Flank instability of Stromboli volcano (Aeolian Islands, Southern Italy): integration of GB-InSAR and geomorphological observations. Geomorphology 201, 60–69.

Keller, J., Hornig-Kjarsgaard, I., Koberski, U., Stadlbauer, E., Lenhart, R., 1993. Geological map of the island of Stromboli. Acta Vulcanol. 3.

La Felice, S., Landi, P., 2011. The 2009 paroxysmal explosions at Stromboli (Italy): magma mixing and eruption dynamics. Bull. Volcanol. 73, 1147–1154.

La Rocca, M., Galluzzo, D., Saccorotti, G., Tinti, S., Cimini, G.B., Del Pezzo, E., 2004. Seismic signals associated with landslides and with a tsunami at Stromboli volcano, Italy. Bull. Seismol. Soc. Am. 94, 1850–1867.

La Spina, A., Burton, M.R., Harig, R., Murè, F., Rusch, P., Jordan, M., Caltabiano, T., 2013. New insights into volcanic processes at Stromboli from Cerberus, a remote-controlled open-path FTIR scanner system. J. Volcanol. Geotherm. Res. 249, 66–76.

Landi, P., Metrich, N., Bertagnini, A., Rosi, M., 2008. Recycling and "re-hydration" of degassed magma inducing transient dissolution/crystallization events at Stromboli (Italy). J. Volcanol. Geotherm. Res. 174, 325–336.

Lautze, N., Houghton, B.F., 2005. Physical mingling of magma and complex eruption dynamics in the shallow conduit at Stromboli volcano, Italy. Geology 33, 425–428.

Lautze, N.C., Houghton, B.F., 2007. Linking variable explosion style and magma textures during 2002 at Stromboli volcano, Italy. Bull. Volcanol. 69, 445–460.

Linde, N., Baron, L., Ricci, T., Finizola, A., Revil, A., Muccini, F., Cocchi, L., Carmisciano, C., 2014. 3D density structure and geological evolution of Stromboli volcano (Aeolian Islands, Italy) inferred from land-based and sea-surface gravity data. J. Volcanol. Geotherm. Res. 273, 58–69.

Lu, Z., Power, J.A., McConnell, V.S., Wicks, C., Dzurisin, D., 2002. Pre- eruptive inflation and surface interferometric coherence characteristics revealed by satellite radar interferometry at Makushin Volcano, Alaska: 1993–2000. J. Geophys. Res. 107 (B11), 2266.

Luzi, G., Del Ventisette, C., Casagli, N., 2010. Monitoring deformations of the Sciara del Fuoco (Stromboli) through ground-based radar interferometry. Acta Vulcanol. 22, 77–84.

Madonia, P., Fiordilino, E., 2013. Time variability of low-temperature fumaroles at Stromboli island (Italy) and its application to volcano monitoring. Bull. Volcanol. 75, 1–12.

Marani, M.P., Gamberi, F., Rosi, M., Bertagnini, A., Di Roberto, A., 2009. Subaqueous density flow processes and deposits of an island volcano landslide (Stromboli Island, Italy). Sedimentology 56, 1488–1504.

Marchetti, E., Genco, R., Ripepe, M., 2009. Ground deformation and seismicity related to the propagation and drainage of the dyke feeding system during the 2007 effusive eruption at Stromboli volcano (Italy). J. Volcanol. Geotherm. Res. 182, 155–161.

Marsella, M., Proietti, C., Sonnessa, A., Coltelli, M., Tommasi, P., Bernardo, E., 2009. The evolution of the Sciara del Fuoco subaerial slope during the 2007 Stromboli eruption: Relation between deformation processes and effusive activity. J. Volcanol. Geotherm. Res. 182, 201–213.

Marsella, M., Baldi, P., Coltelli, M., Fabris, M., 2012. The morphological evolution of the Sciara del Fuoco since 1868: reconstructing the effusive activity at Stromboli volcano. Bull. Volcanol. 74, 1–18.

Martini, M., Giudicepietro, F., D'Auria, L., Esposito, A.M., Caputo, T., Curciotti, R., De Cesare, W., Orazi, M., Scarpato, G., Caputo, A., Peluso, R., Ricciolino, P., Linde, A., Sacks, S., 2007. Seismological monitoring of the February 2007 effusive eruption of the Stromboli volcano. Ann. Geofis. 50, 775–788.

Mattia, M., Rossi, M., Guglielmino, F., Aloisi, M., Bock, Y., 2004. The shallow plumbing system of Stromboli Island as imaged from 1 Hz instantaneous GPS positions. Geophys. Res. Lett. 31 (24).

Métrich, N., Bertagnini, A., Di Muro, A., 2010. Conditions of magma storage, degassing and ascent at Stromboli: new insights into the volcano plumbing system with inferences on the eruptive dynamics. J. Petrol. 51, 603–626.

Nave, R., Isaia, R., Vilardo, G., Barclay, J., 2010. Re-assessing volcanic hazard maps for improving volcanic risk communication: application to Stromboli Island, Italy. J. Maps 6, 260–269.

Neri, M., Lanzafame, G., 2009. Structural features of the 2007 Stromboli eruption. J. Volcanol. Geotherm. Res. 182, 137–144.

Neri, M., Lanzafame, G., Acocella, V., 2008. Dyke emplacement and related hazard in volcanoes with sector collapse: the 2007 Stromboli (Italy) eruption. J. Geol. Soc. 165, 883–886.

Newhall, C.G., Self, S., 1982. The Volcanic Explosivity Index (VEI) an estimate of explosive magnitude for historical volcanism. J. Geophys. Res. Oceans (1978–2012) 87 (C2), 1231–1238.

Nolesini, T., Di Traglia, F., Del Ventisette, C., Moretti, S., Casagli, N., 2013. Deformations and slope instability on Stromboli volcano: integration of GBInSAR data and analogue modeling. Geomorphology 180–181, 242–254.

Parfitt, E.A., 2004. A discussion of the mechanisms of explosive basaltic eruptions. J. Volcanol. Geotherm. Res. 134, 77–107.

Patrick, M., Harris, A.J.L., Ripepe, M., Dehn, J., Rothary, D.A., Calvari, S., 2007. Strombolian explosive styles and source conditions: insights from thermal (FLIR) video. Bull. Volcanol. 69, 769–784.

Pinel, V., Jaupart, C., 2004. Magma storage and horizontal dyke injection beneath a volcanic edifice. Earth Planet. Sci. Lett. 221, 245–262.

Pioli, L., Pistolesi, M., Rosi, M., 2014. Transient explosions at open-vent volcanoes: The case of Stromboli (Italy). Geology 42 (10), 863–866.

Pistolesi, M., Rosi, M., Pioli, L., Renzulli, A., Bertagnini, A., Andronico, D., 2008. The paroxysmal explosion and its deposits. In: Calvari, S., Inguaggiato, S., Puglisi, G., Ripepe, M., Rosi, M. (Eds.), The Stromboli volcano: An integrated study of the 2002–2003 eruption. American Geophysical Union Monograph Series 182, pp. 317–329.

Pistolesi, M., Delle Donne, D., Pioli, L., Rosi, M., Ripepe, M., 2011. The 15 March 2007 explosive crisis at Stromboli volcano, Italy: assessing physical parameters through a multidisciplinary approach. J. Geophys. Res. 116, B12206.

Puglisi, G., Bonaccorso, A., Mattia, M., Aloisi, M., Bonforte, A., Campisi, O., Cantarero, M., Falzone, G., Puglisi, B., Rossi, M., 2005. New integrated geodetic monitoring system at Stromboli volcano (Italy). Eng. Geol. 79 (1), 13–31.

Renzulli, A., Del Moro, S., Menna, M., Landi, P., Piermattei, M., 2009. Transient processes in Stromboli's shallow basaltic system inferred from dolerite and magmatic breccia blocks erupted during the 5 April 2003 paroxysm. Bull. Volcanol. 71 (7), 795–813.

Rivalta, E., Pascal, K., Phillips, J., Bonaccorso, A., 2013. Explosive expansion of a slowly decompressed magma: Evidence for delayed bubble nucleation. Geochem. Geophys. Geosyst. 14. http://dx.doi.org/10.1002/ggge.20183.

Roche, O., Wyk, Van, de Vries, B., Druitt, T.H., 2001. Sub-surface structures and collapse mechanisms of summit pit craters. J. Volcanol. Geotherm. Res. 105 (1), 1–18.

Romagnoli, C., Kokelaar, P., Casalbore, D., Chiocci, F.L., 2009. Lateral collapses and active sedimentary processes on the northwestern flank of Stromboli volcano. Mar. Geol. 265, 101–119.

Rosi, M., 1980. The Island of Stromboli. Rend. Soc. Ital. Mineral. Petrol. 36, 345–368.

Rosi, M., Bertagnini, A., Landi, P., 2000. Onset of the persistent activity at Stromboli volcano (Italy). Bull. Volcanol. 62, 294–300.

Rosi, M., Bertagnini, A., Harris, A.J.L., Pioli, L., Pistolesi, M., Ripepe, M., 2006. A case history of paroxysmal explosion at Stromboli: timing and dynamics of the April 5, 2003 event. Earth Planet. Sci. Lett. 243, 594–606.

Rosi, M., Pistolesi, M., Bertagnini, A., Landi, P., Pompilio, M., Di Roberto, A., 2013. Aeolian Islands (Italy): present eruptive activity and hazards. Geol. Soc. Lond. Mem. 37, 473–490.

Rotonda, T., Tommasi, P., Boldini, D., 2010. Geomechanical characterization of the volcaniclastic material involved in the 2002 landslides at Stromboli. J. Geotech. Geoenviron. Eng. 136, 239–401.

Rubin, A.M., 1995. Propagation of magma-filled cracks. Annu. Rev. Earth Planet. Sci. 23, 287–336.

Ruch, J., Pepe, S., Casu, F., Acocella, V., Neri, M., Solaro, G., Sansosti, E., 2012. How do volcanic rift zones relate to flank instability? Evidence from collapsing rifts at Etna. Geophys. Res. Lett. 39 (20).

Speranza, F., Pompilio, M., D'Ajello Caracciolo, F., Sagnotti, L., 2008. Holocene eruptive history of the Stromboli volcano: constraints from paleomagnetic dating. J. Geophys. Res. Solid Earth (1978–2012) 113 (B9).
Taddeucci, J., Scarlato, P., Capponi, A., Del Bello, E., Cimarelli, C., Palladino, D.M., Kueppers, U., 2012. High- speed imaging of Strombolian explosions: the ejection velocity of pyroclasts. Geophys. Res. Lett. 39, L02301.
Taddeucci, J., Palladino, D.M., Sottili, G., Bernini, D., Andronico, D., Cristaldi, A., 2013. Linked frequency and intensity of persistent volcanic activity at Stromboli (Italy). Geophys. Res. Lett. 40 (13), 3384–3388.
Tarchi, D., Casagli, N., Fortuny-Guassch, J., Guerri, L., Antonello, G., Leva, D., 2008. Ground deformation from ground-based SAR interferometry. In: Calvari, S., Inguaggiato, S., Puglisi, G., Ripepe, M., Rosi, M. (Eds.), The Stromboli volcano: An integrated study of the 2002–2003 eruption. American Geophysical Union Monograph Series 182, 359–372, pp. 359–372.
Ter-Stepanian, G., 1966. Types of depth creep of slopes in rock masses. Proc. First Congress Int. Soc. Rock Mechanics, Lisbon 2, pp. 157–160.
Thomas, M.E., Petford, N., Bromhead, E.N., 2004. Volcanic rock-mass properties from Snowdonia and Tenerife: implications for volcano edifice strength. J. Geol. Soc. 161 (6), 939–946.
Tibaldi, A., 2001. Multiple sector collapses at Stromboli volcano, Italy: how they work. Bull. Volcanol. 63 (2–3), 112–125.
Tibaldi, A., 2003. Influence of cone morphology on dykes, Stromboli, Italy. J. Volcanol. Geotherm. Res. 126, 79–95.
Tibaldi, A., Apuani, T., Corazzato, C., Pasquaré, F.A., Vezzoli, L., 2008. Geological–structural framework of Stromboli Volcano, past collapses, and the possible influence on the events of the 2002–03 crisis. AGU Monogr. 182.
Tibaldi, A., Corazzato, C., Marani, M., Gamberi, F., 2009. Subaerial–submarine evidence of structures feeding magma to Stromboli Volcano, Italy, and relations with edifice flank failure and creep. Tectonophysics 469, 112–136.
Tinti, S., Manucci, A., Pagnoni, G., Armigliato, A., Zaniboni, F., 2005. The 30 December 2002 landslide-induced tsunamis in Stromboli: sequence of events reconstructed from the eyewitness accounts. Nat. Hazards Earth Syst. Sci. 5, 763–775.
Tinti, S., Pagnoni, G., Zaniboni, F., 2006. The landslides and tsunamis of the 30th of December, 2002 in Stromboli analysed through numerical simulations. Bull. Volcanol. 68, 462–479.
Tommasi, P., Baldi, P., Chiocci, F.L., Coltelli, M., Marsella, M., Pompilio, M., Romagnoli, C., 2005. The landslide sequence induced by the 2002 eruption at Stromboli volcano. In: Sassa, K., Fukuoka, H., Wang, F.W., Wang, G. (Eds.), Landslide-risk analysis and sustainable disaster management. Springer, New York, pp. 251–258.
Vergniolle, S., Brandeis, G., 1996. Strombolian explosions: 1. A large bubble breaking at the surface of a lava column as a source of sound. J. Geophys. Res. Solid Earth (1978–2012) 101 (B9), 20433–20447.
Vezzoli, L., Renzulli, A., Menna, M., 2014. Growth after collapse: the volcanic and magmatic history of the Neostromboli lava cone (island of Stromboli, Italy). Bull. Volcanol. 76 (6), 1–24.
Voight, B., Elsworth, D., 1997. Failure of volcano slopes. Geotechnique 47, 1–31.
Vona, A., Romano, C., Dingwell, D.B., Giordano, D., 2011. The rheology of crystal-bearing basaltic magmas from Stromboli and Etna. Geochim. Cosmochim. Acta 75, 3214–3236.
Witham, F., 2011. Conduit convection, magma mixing, and melt inclusion trends at persistently degassing volcanoes. Earth Planet. Sci. Lett. 301 (1), 345–352.